Nature and Science of Sleep

Elevate Series

Open Access Full Text Article

ORIGINAL RESEARCH

Metabolomic Biomarkers for Non-Invasive Diagnosis of Coronary Artery Disease and Obstructive Sleep Apnea Co-Occurrence

Shuhan Chen[1,*], Qingquan Liu[1,*], Jing Liu[1], Huijuan Zheng[1], Wanqi Li[1], Liying Yu[2,3]

[1]Cardiovascular Medicine, The Second Affiliated Hospital of Fujian Medical University, Quanzhou, 362000, People's Republic of China; [2]Central Laboratory, Fujian Key Laboratory of Lung Stem Cells, The Second Affiliated Hospital of Fujian Medical University, Quanzhou, 362000, People's Republic of China; [3]Department of Bioinformatics, School of Medical Technology and Engineering, School of Medical Imaging, Fujian Medical University, Fuzhou, Fujian, 350122, People's Republic of China

*These authors contributed equally to this work

Correspondence: Liying Yu, Email yly@fjmu.edu.cn

Nature and Science of Sleep downloaded from https://www.dovepress.com/
For personal use only.

Background and Aims: The comorbid state of obstructive sleep apnea (OSA) and coronary artery disease (CAD) has emerged as a significant public health challenge. However, the underlying metabolic regulation and molecular biomarkers linking to the CAD and OSA comorbidity (CADOSA) remain poorly understood. This study aimed to identify non-invasive biomarkers for the CADOSA comorbidity.

Methods: We randomly recruited a total of 143 participants from a hospital-based setting, comprising four groups: healthy controls (n=38), patients with OSA-only (n=37), CAD-only (n=36), and comorbid CADOSA (n=32). Participants were predominantly male (69.2%), with a mean age of 59.44 years (SD 12.25) and 24.77±3.94 BMI index. Comprehensive clinical evaluation and blood metabolomic profiling were conducted. We integrated differential expression analysis, functional enrichment, machine learning, receiver operating characteristic (ROC) curve, and matched transcriptomes association analysesto uncover key metabolites and potential molecular regulatory mechanisms associated with CADOSA.

Results: Baseline clinical data revealed that CADOSA comorbidity significantly exacerbates more severe cardiac dysfunction and sleep disordered breathing than two unique disease stages, despite no significant differences in age or BMI among the groups. Common disordered metabolites in patients with OSA-only or CAD-only were primarily associated with fatty acid, steroid, amino acid, and energy metabolism. While OSA-specific metabolic pathways included ascorbate and aldarate metabolism, alpha-linolenic acid metabolism, and primary bile acid biosynthesis. In contract, CAD specific pathways consisted of arginine biosynthesis, sphingolipid metabolism, pyruvate metabolism, and glycerophospholipid metabolism. Specifically, CADOSA patients exhibited unique metabolic pathways involving unsaturated fatty acid biosynthesis. Machine learning analysis identified the newly discovered and top-ranking potential metabolomic biomarkers for each condition: upregulated D-glucuronolactone for OSA, increased 12-hydroxyoctadecanoic acid for CAD, and downregulated tryptophan for CADOSA. Matched transcriptome association analysis revealed highly expressed and strongly correlated metabolite-gene pairs in the CADOSA comorbidity, including tryptophan-DMXL2, (C12-AE1S)-ZDHHC11, and IBMX-FCAR, which acting as potential up- and down-stream regulatory relationships underlying progress of CADOSA.

Conclusion: This study elucidates the distinct clinical features and metabolic profiles of OSA, CAD, and comorbid CADOSA. These newly identified metabolic biomarkers and associative gene-metabolite pairs highlight a distinct comorbidity-specific metabolic and transcriptional architectures, providing novel insights into the development of molecular biomarkers and therapeutic targets for CADOSA.

Keywords: metabolomics, coronary artery disease, obstructive sleep apnea, machine learning

Introduction

Obstructive sleep apnea (OSA), marked by recurrent upper airway collapse during sleep, triggers intermittent hypoxia (IH) and heightened sympathetic activity. Epidemiological data indicate a prevalence of 17% in women and 34% in men,

https://doi.org/10.2147/NSS.S575902
Received: 14 November 2025
Accepted: 10 February 2026
Published: 10 March 2026

© 2026 Chen et al. This work is published and licensed by Dove Medical Press Limited. The full terms of this license are available at https://www.dovepress.com/terms.php and incorporate the Creative Commons Attribution – Non Commercial (unported, v4.0) License (http://creativecommons.org/licenses/by-nc/4.0/). By accessing the work you hereby accept the Terms. Non-commercial uses of the work are permitted without any further permission from Dove Medical Press Limited, provided the work is properly attributed. For permission for commercial use of this work, please see paragraphs 4.2 and 5 of our Terms (https://www.dovepress.com/terms.php).

with OSA recognized as an independent risk factor for coronary artery disease (CAD).[1,2] Despite its clinical significance, OSA often remains underdiagnosed due to subtle early symptoms, underscoring the need for early detection. In China, cardiovascular diseases affect 330 million individuals, with CAD being the predominant contributor to mortality and healthcare burden.[3] CAD pathogenesis involves lipid plaque accumulation in coronary arteries, leading to stenosis and cardiac dysfunction. Notably, OSA prevalence is significantly elevated among CAD patients, suggesting a bidirectional relationship.[4,5] The frequent co-occurrence of OSA and CAD exacerbates disease progression through shared pathophysiological mechanisms, resulting in poorer clinical outcomes.[6–9] Moreover, the utility of clinical risk stratification in OSA is underscored by recent evidence demonstrating that patients categorized as high-risk by the NoSAS score carry a significantly greater burden of cardiovascular disease.[10] Despite increasing recognition of their comorbidity (CADOSA) as a high-risk phenotype, no validated non-invasive biomarkers exist for early detection or risk stratification.

In our previous transcriptomic study, we characterized the gene expression profiles in peripheral blood mononuclear cells (PBMCs) from patients with CAD, OSA, and their comorbidity, identifying key dysregulated pathways and potential genetic biomarkers such as S100A12 and MMP9.[11] While that study provided crucial insights into the genomic underpinnings of CADOSA, gene expression profiles primarily reflect the potential for cellular activity rather than the final functional outcome. In contrast, metabolomics offers a more direct snapshot of the functional activity and the downstream effects of genetic and environmental influences, serving as a bridge between genomics, transcriptomics, and proteomics. This approach has significantly advanced disease biomarker discovery, therapeutic target identification, and metabolic pathway analysis.[12–14] Although previous studies have reported overlapping metabolic alterations or biomarkers in OSA and CAD individually, a comprehensive metabolic profile specific to their comorbidity remains unexplored. For example, in OSA, metabolomic analyses have revealed disturbances not only in glucose and lipid metabolism but also in amino acid and purine metabolism, along with gut microbiota-derived metabolites. Time-series blood analyses demonstrate significant changes in amino acids and biogenic amines,[15–17] while intermittent hypoxia alters the Firmicutes/Bacteroidetes ratio, elevates reactive oxygen species (ROS), and free fatty acids (FFA),[18] and reduces porphyrin and glycerophospholipid (GPL) expression in severe OSA.[19] Glutamate and phenylalanine have been suggested as biomarkers for OSA.[20] In CAD, beyond traditional markers such as low-density lipoprotein cholesterol (LDL-C) and C-reactive protein (CRP),[21] emerging metabolic signatures include dysregulated tricarboxylic acid cycle intermediates during ischemia,[22] alterations in sphingomyelins, tryptophan levels associated with CAD severity,[23,24] and gut microbiota-derived dysregulated short-chain fatty acids (SCFAs) with immunomodulatory roles.[25] Although preliminary evidence suggests that certain metabolites—such as urinary epinephrine sulfate,[26] serum phospholipase A1 and sphingomyelins,[27] and microbiota-produced bile acids[15]—may link OSA to increased cardiovascular risk, most existing research, including our prior transcriptomic study,[11] has focused on single-disease or single-omics analyses. Therefore, a comprehensive metabolomic investigation of CADOSA comorbidity is imperative to uncover the functional metabolic perturbations and to identify non-invasive biomarkers that complement transcriptomic findings.

In this study, we performed comparative metabolomic profiling via high-resolution liquid chromatography-mass spectrometry (LC-MS) combined with bioinformatics and machine learning to characterize serum metabolic signatures and identify biomarkers in OSA-only, CAD-only, and CADOSA patients versus healthy controls. To enhance the clinical relevance and robustness of our findings, we have expanded the patient cohort compared to our previous transcriptomic study.[11] Integrated metabolome-transcriptome analysis further revealed gene–metabolite interaction networks, uncovering potential regulatory mechanisms in CADOSA. These findings advance the understanding of CADOSA pathogenesis and may facilitate the development of noninvasive biomarker panels for early diagnosis, risk stratification, and personalized therapeutic strategies.

Materials and Methods

Study Cohort and Clinical Assessment

This metabolomic investigation received ethical approval from the Institutional Review Board, with all subjects providing written informed consent. All participants underwent comprehensive clinical characterization and disease confirmation using the same rigorous criteria detailed in our prior transcriptomic investigation.[11] In brief, CAD and OSA

were definitively diagnosed by specialist consensus using coronary angiography and polysomnography, respectively. The present metabolomic analysis extends this work through a significantly expanded cohort of 143 participants, enhancing the statistical power of our findings. The final analytical cohort was systematically categorized into four distinct clinical groups: 36 patients with CAD, 37 with OSA, 32 with CAD and OSA comorbidity (CADOSA), and 38 healthy controls.

Plasma Acquisition and Metabolite Isolation

Peripheral venous blood was collected from all participants after an overnight fast and transferred into EDTA-anticoagulated Vacutainer tubes (5 mL; BD Biosciences). Plasma was separated by centrifugation at 1,500 ×g for 15 min at 4°C and stored at −80°C until analysis. For metabolite extraction, 100 μL of thawed plasma was mixed with 400 μL of ice-cold methanol/acetonitrile (1:1, v/v) via vortexing. The mixture was incubated at −20°C for 1 h and then centrifuged at 14,000 ×g for 20 min (4°C). The resulting supernatant was lyophilized using a SpeedVac concentrator (Thermo Fisher Scientific). The dried extract was reconstituted in 100 μL of acetonitrile/water (1:1, v/v), followed by centrifugation at 14,000 ×g for 15 min at 4°C. The clarified supernatant was transferred into LC-MS vials for analysis. A pooled quality control (QC) sample was prepared by combining 10 μL aliquots from each individual sample. QC samples were injected after every five experimental samples to assess instrumental performance and stability.

Metabolic Profiling Using LC-MS/MS

LC-MS/MS analysis was conducted on an ultra-high performance liquid chromatography system (1290 Infinity LC, Agilent Technologies) coupled with a quadrupole time-of-flight mass spectrometer (AB SCIEX Triple TOF 5600) at Guangzhou Verygenome Technology Co., Ltd. Chromatographic separation was achieved using a HILIC-based ACQUITY UPLC BEH Amide column (2.1 mm × 100 mm, 1.7 μm; Waters, Ireland) maintained at 40°C. The mobile phase consisted of (A) 25 mM ammonium acetate and 25 mM ammonium hydroxide in water and (B) acetonitrile. The gradient elution program was operated at a flow rate of 0.3 mL/min as follows: 95% B (0–0.5 min), linearly decreased to 65% B (6.5 min), further reduced to 40% B (7.5 min), held at 40% B (8.5 min), rapidly increased to 95% B (8.6 min), and finally re-equilibrated at 95% B for 3 min (total run time: 11.6 min).

Mass spectrometric measurements were performed in both ESI polarities. Source conditions comprised: nebulizing and auxiliary gas at 60 psi each, curtain gas at 30 psi, temperature of 600°C, and spray voltage of ±5.5 kV. Full-scan data (m/z 60–1000 Da; 0.20 s/spectrum) were acquired in TOF mode. Automated MS/MS was performed via an IDA method, acquiring fragmentation spectra (m/z 25–1000; 0.05 s/spectrum) with a collision energy of 35 ± 15 eV. Declustering potentials were ±60 V depending on polarity. The data-dependent acquisition employed a 4 Da isotope exclusion and a 10-ion-per-cycle limit to optimize the fragmentation strategy.

Metabolomics Data Processing

Raw data were converted to mzXML format by MSConvert. Peak detection and alignment were conducted in XCMS (centWave: 10 ppm; peak width: 10–60 s; prefilter: [10, 100]). The resulting features were grouped (retention time tolerance: 5 s; mass tolerance: 0.025 Da; minfrac 0.5) and filtered to retain those present in >50% of samples in any group. Isotope and adduct annotation used CAMERA (Collection of Algorithms of Metabolites Profile Annotation). Metabolites were identified by matching accurate mass (<10 ppm error) and MS/MS spectra to a custom library of authentic standards.

Identification and Functional Analysis of Differentially Expressed Metabolites

After data quality control and normalization, multivariate statistical analyses were conducted using the ropls package in R. Differential metabolites were identified based on thresholds of $|\log_2 FC| \geq 1$, adjusted $p<0.05$, and variable importance in projection (VIP) ≥ 1. Unsupervised principal component analysis (PCA), supervised partial least squares-discriminant analysis (PLS-DA), and volcano plots were utilized to assess inter-group metabolic variations and visualize differentially expressed metabolites. Model robustness was validated through sevenfold cross-validation and permutation testing. Pathway enrichment analysis was performed using the Kyoto Encyclopedia of Genes and Genomes (KEGG) database, with pathways meeting adjusted $p<0.05$ considered statistically significant.

Diagnostic Model Development Using Machine Intelligence

The participant cohort was randomly partitioned into training (70%) and validation (30%) subsets. Three machine learning approaches were implemented to construct diagnostic classifiers: elastic net regression for its robustness to multicollinearity (with the regularization parameter λ set to 0.05); random forest algorithms evaluating feature importance through mean decrease Gini indices; and support vector machine models. To enhance model robustness and generalizability, all classifiers were trained and validated using a repeated 10-fold cross-validation strategy. The five most predictive metabolite features, determined by consensus ranking across methods, were incorporated into final classification models. The predictive performance was evaluated using receiver operating characteristic (ROC) curves, illustrating the relationship between sensitivity and 1–specificity. Diagnostic accuracy was determined by the area under the ROC curve (AUC), where values closer to 1.0 indicate better discriminative ability and fewer misclassifications.

Cross-Omics Integration Analysis

To investigate inter-omics relationships, metabolite profiles were integrated with matched gene expression data from our previous investigation. Pairwise correlation coefficients were computed between key diagnostic metabolites and all differentially expressed genes. Statistically significant associations ($R>0.4$, $p<0.05$) were used to construct gene–metabolite interaction networks, with visualization implemented in Cytoscape.[28]

Clinical Data Statistical Evaluation

Clinical parameter analysis was performed using SPSS statistical software. Continuous variables were summarized as mean ± standard deviation or median with interquartile range according to distribution characteristics. Categorical variables were presented as frequencies and percentages. Intergroup comparisons employed parametric or nonparametric methods based on data distribution properties, with two-tailed $p<0.05$ considered statistically significant.

Results

Cohorts Characteristics

The baseline clinical profiles of all participants are summarized in Supplementary Table S1. No significant differences were observed across the four groups (38 healthy controls, 37 OSA-only, 36 CAD-only, and 32 CADOSA) in age, BMI, heart rate, or key blood biochemistry indexes. However, as detailed in Table 1, each patient group exhibited a distinct clinical profile relative to healthy controls. Patients with OSA alone presented with elevated diastolic blood pressure and increased red blood cell counts, consistent with sympathetic activation and compensatory erythropoiesis. In contrast, the CAD group was marked by a significant rise in NT-proBNP, indicating pronounced cardiac strain. Patients with comorbid CAD and OSA (CADOSA) demonstrated the most pronounced cardiac remodeling, as evidenced by enlarged left ventricular dimensions. As expected, both the OSA and CADOSA groups exhibited severe nocturnal hypoxia, reflected in substantially higher AHI and lower SpO_2. Collectively, these findings delineate the unique and shared pathophysiological features across the disease spectrum.

Overall Metabolomic Data Quality and Model Reliability

Plasma samples from HC, OSA, CAD, and CADOSA groups underwent metabolite preprocessing and identification, retaining ≥ level 21,385 metabolites. The overlapping total ion current chromatograms exhibit consistent peak intensities and retention times across repeated quality control samples (Supplementary Figure S1), demonstrating minimal instrumental variability and excellent signal stability. Pearson correlation (Supplementary Figure S2) and PCA (Supplementary Figure S3) results of all QC samples further confirmed exceptional reproducibility.

PCA and OPLS-DA analyses revealed clear separation between each pairwise groups. The OSA vs HC comparison yielded R2Y=0.932 and Q2=0.928 (Figure 1A), CAD vs HC showed R2Y=0.851 and Q2=0.841 (Figure 1B), CADOSA vs HC exhibited R2Y=0.607 and Q2=0.555 (Figure 1C), CADOSA vs OSA demonstrated R2Y=0.862 and Q2=0.88 (Figure 1D), and CADOSA vs CAD displayed R2Y=0.781 and Q2=0.819 (Figure 1E). All model parameters (R2Y and Q2≥0.5) indicated robust model reliability. Permutation tests confirmed the absence of overfitting in these models.

Table 1 Demographic and Clinical Characteristics of the Participants at Baseline

Characteristic	HC n=38	OSA n=37	CAD n=36	CADOSA n=32	P value	Comparison[#]
Gender*					0.008	
Male, n (%)	19(50%)	27(73%)	25(69.4%)	28(87.5%)		
Female, n (%)	19(50%)	10(27%)	11(30.6%)	4(12.5%)		
DBP*, mmHg	79.24±10.79	88.22±16.53	84.70±11.85	80.27±11.47	0.017	1<2 4<2
RBC*, 10^{12}/L	4.56±0.48	4.88±0.58	4.53±0.49	4.53±0.62	0.021	1, 3, 4<2
NT-proBNP*, pg/mL	82.9(41.3,274.6)	55.5(29.7,122.3)	151.3(77,726.3)	60.1(17.8,236.7)	0.011	1, 2<3
LVD*, mm	47(43.5,48.5)	47(43.8,49.3)	49(44.3,49.8)	48(47,51)	0.026	1<4
LVS*, mm	30(28,31)	29.5(27.75,32)	30(27.25,31)	31(30,33)	0.005	1, 2<4
Left ventricular hypertrophy*					0.036	
Yes, n (%)	4(10.5%)	11(29.7%)	11(30.6%)	13(40.6%)		
No, n (%)	34(89.5%)	26(70.3%)	25(69.4%)	19(59.4%)		
AHI*, events/h	1.95(1.1,4.3)	15.2(11.4,24.3)	3.9(1,4.2)	19.4(9.2,34.2)	<0.01	1<2, 4 3<2, 4
SpO_2*, %	89(85.8,90.8)	83(80,85)	89(88,91)	84(78,88)	0.002	2<1, 3 4<3

Notes: Values are mean ± SD, n (%), or median (interquartile range), unless otherwise indicated. Differences in clinical and imaging parameters between groups were compared using one-way ANOVA. "*" marks a significant difference in the clinical factor among the HC, OSA, CAD, and CADOSA groups ($p<0.05$). "#" LSD (Least Significant Difference) method or T2 method or Bonferroni method was used for pairwise comparison within groups,1=HC, 2=OSA, 3=CAD, 4=CADOSA.
Abbreviations: n, number of patients; DBP, diastolic blood pressure; RBC, red blood cells; NT-proBNP, N-terminal pro-B-type natriuretic peptide; LVD, left ventricular end-diastolic diameter; LVS, left ventricular end-systolic diameter; AHI, apnea hyponea index; SpO_2, peripheral oxygen saturation.

Metabolic Profiling of OSA and CAD

The metabolomic differential analysis revealed that the OSA group exhibited 385 differentially expressed metabolites (adjusted $p<0.05$) compared to the HC group, among which 171 were upregulated. The top five most significantly upregulated metabolites were kuwanon C, 3-O-methylgallic acid, bufalin, cynarin, and urobilinogen. Meanwhile, 214 metabolites were downregulated, with the top five most significantly downregulated being dipropyl phthalate, CMPF, phomalone, ethylbeta-carboline, and oleic acid (Supplementary Table S2). The functional classification analysis shows that approximately 59% of these differential metabolites belong to fatty acids and conjugates, steroids, sterols, isoprenoids, and amino acids and peptides (listed in decreasing order). KEGG enrichment analysis indicated that the top 10 pathways significantly associated with these differential metabolites included biosynthesis of unsaturated fatty acids, steroid hormone biosynthesis, citrate cycle (TCA cycle), alanine, aspartate and glutamate metabolism, ascorbate and aldarate metabolism, tyrosine metabolism, primary bile acid biosynthesis, fatty acid biosynthesis, phenylalanine metabolism, and alpha-linolenic acid metabolism (Figure 2A).

In comparison with the HC group, the CAD group displayed 295 differentially expressed metabolites (adjusted $p<0.05$), comprising 106 upregulated and 189 downregulated metabolites. The top five upregulated metabolites were kuwanon C, methyl 3-(4-hydroxy-6-methyl-2-oxo-2H-pyran-3-yl)-3-phenylpropanoate, bufalin, boscalid, and urobilinogen, while the top five downregulated metabolites were phomalone, oleic acid, dipropyl phthalate, CMPF, and cimifugin (Supplementary Table S3). Functional classification revealed that approximately 54% of these differential metabolites were categorized as fatty acids and conjugates, steroids, amino acids and peptides, and isoprenoids and sterols. KEGG enrichment analysis demonstrated that the top 10 enriched pathways in the CAD group included biosynthesis of unsaturated fatty acids, steroid hormone biosynthesis, tyrosine metabolism, fatty acid biosynthesis, arginine biosynthesis, citrate cycle (TCA cycle), sphingolipid metabolism, pyruvate metabolism, alanine, aspartate and glutamate metabolism, and glycerophospholipid metabolism (Figure 2B).

A Venn diagram was generated based on the pairwise comparison data to identify shared and distinct metabolic pathways. The results showed that six metabolic pathways were common to both CAD and OSA, while each group also exhibited four unique pathways. OSA-specific pathways included ascorbate and aldarate metabolism, phenylalanine

https://doi.org/10.2147/NSS.S575902

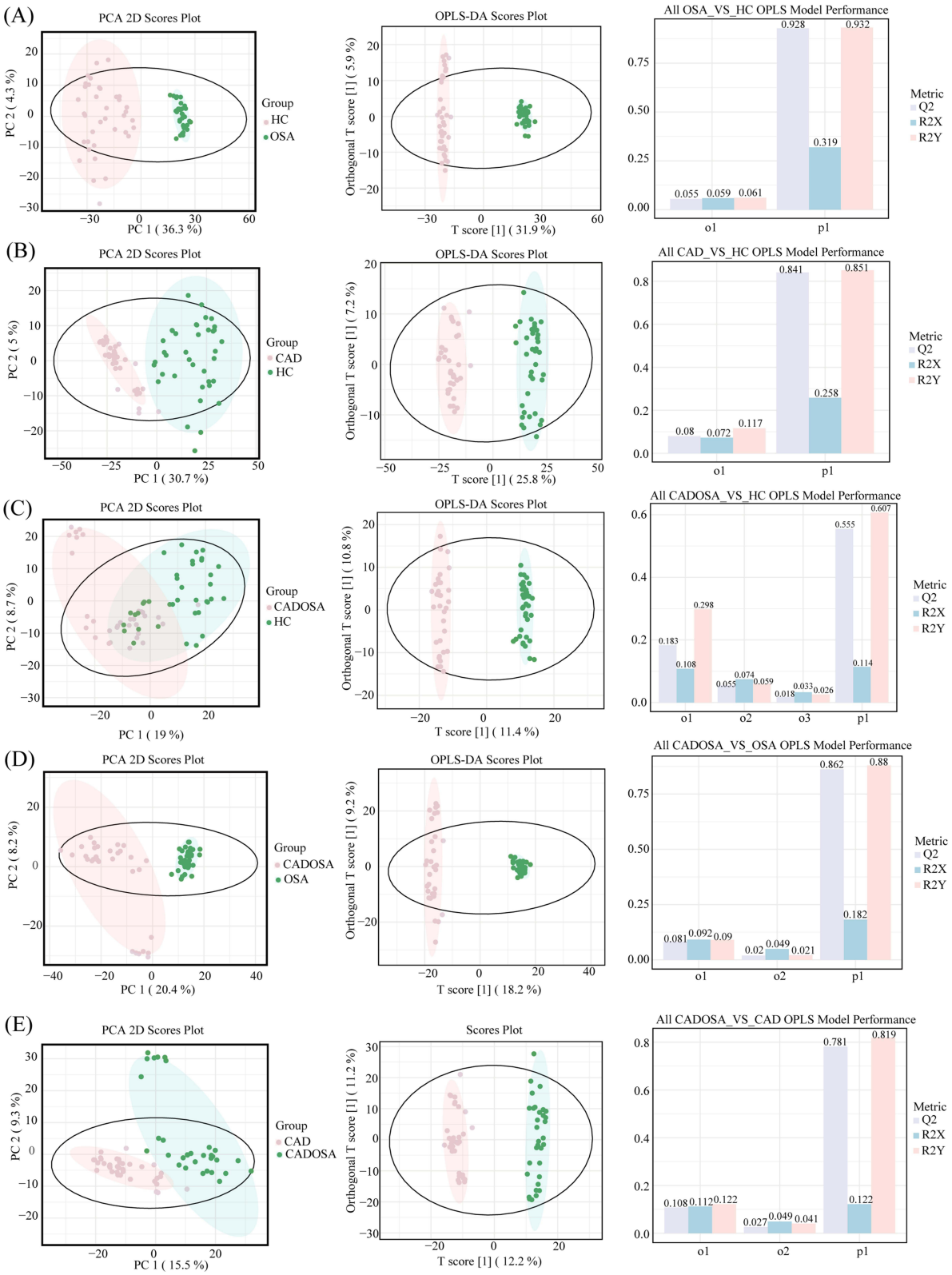

Figure 1 Pairwise comparative analysis among the HC, OSA, CAD, and CADOSA groups. (**A**) From left to right: PCA score plot of OSA vs HC, OPLS-DA score plot, and model validation plot displaying evaluation metrics (R2Y, Q2). (**B**) From left to right: PCA score plot of CAD vs HC, OPLS-DA score plot, and model validation plot displaying evaluation metrics (R2Y, Q2). (**C**) From left to right: PCA score plot of CADOSA vs HC, OPLS-DA score plot, and model validation plot displaying evaluation metrics (R2Y, Q2). (**D**) From left to right: PCA score plot of CADOSA vs OSA, OPLS-DA score plot, and model validation plot displaying evaluation metrics (R2Y, Q2). (**E**) From left to right: PCA score plot of CADOSA vs CAD, OPLS-DA score plot, and model validation plot displaying evaluation metrics (R2Y, Q2).

https://doi.org/10.2147/NSS.S575902

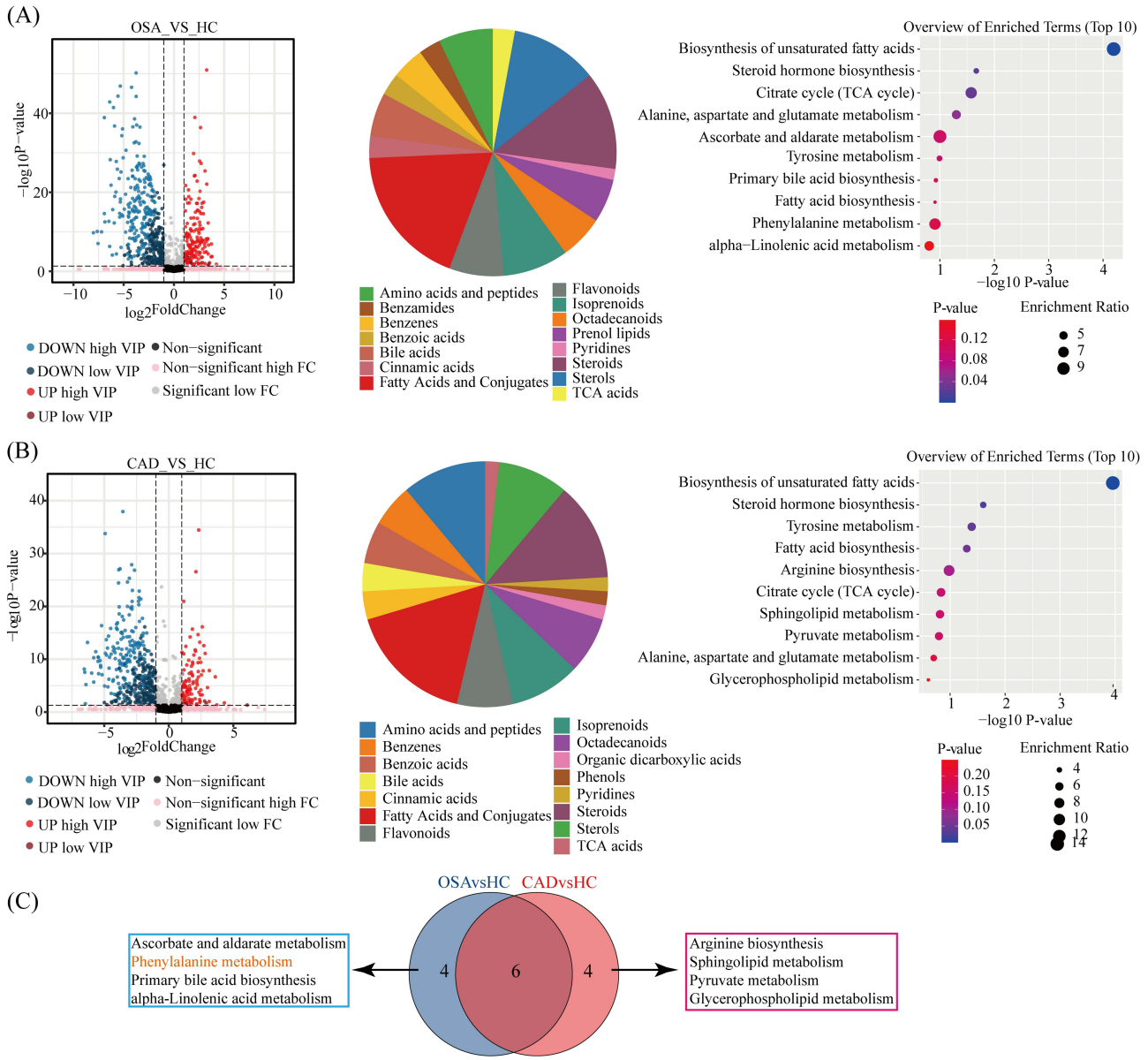

Figure 2 Differential metabolite analysis between OSA or CAD and healthy control groups. (**A**) Volcano plot displays differentially expressed metabolites in OSA compared to HC, where green dots represent downregulated metabolites and red dots indicate upregulated metabolites. The pie chart illustrates functional classification of the differential metabolites. Bubble plot shows the top 10 KEGG pathways enriched by the differential metabolites. (**B**) Volcano plot presents differentially expressed metabolites in CAD versus HC, with green dots denoting downregulated metabolites and red dots indicating upregulated metabolites. The pie chart demonstrates functional categorization of the differential metabolites. Bubble plot displays the top 10 KEGG pathways enriched by the differential metabolites. (**C**) Venn diagram illustrates overlapping and group-specific pathways between OSA vs HC and CAD vs HC.

metabolism, primary bile acid biosynthesis, and alpha-linolenic acid metabolism. In contrast, CAD-specific pathways comprised arginine biosynthesis, sphingolipid metabolism, pyruvate metabolism, and glycerophospholipid metabolism (Figure 2C).

Metabolic Landscape of CADOSA Morbidity

To comprehensively characterize the key metabolites associated with CADOSA comorbidity, we performed three distinct differential comparison analyses: CADOSA versus HC, CADOSA versus CAD, and CADOSA versus OSA. Relative to the HC group, the CADOSA group exhibited 162 differentially expressed metabolites (adjusted $p<0.05$), comprising 44 upregulated and 118 downregulated metabolites. The most significantly upregulated metabolites included tryptophan,

https://doi.org/10.2147/NSS.S575902

fumonisin_B1, [6]-shogaol, pseudojervine, and kuwanon C, while the top five downregulated metabolites were PI 34:2, PI 36:4, PG 36:4, 2,3-dihydroxypropyl stearate, and phenylethylamide 359 (Supplementary Table S4). Metabolite classification revealed that approximately 57% belonged to structural classes including fatty acids and conjugates, steroids, flavonoids, octadecanoids, and sterols. KEGG pathway enrichment analysis demonstrated that these differential metabolites were primarily associated with ten key metabolic pathways: biosynthesis of unsaturated fatty acids, phenylalanine metabolism, alpha-linolenic acid metabolism, arachidonic acid metabolism, fatty acid elongation, fatty acid degradation, tryptophan metabolism, fatty acid biosynthesis, aminoacyl-tRNA biosynthesis, and steroid hormone biosynthesis (Figure 3A).

The CADOSA versus OSA comparison identified 353 differential metabolites (203 upregulated, 150 downregulated, adjusted $p<0.05$). The most markedly upregulated metabolites were tryptophan, O,O-diethyl_phosphate, tebufenozide, 1-[8-hydroxy-3-methyl-1-[(2S,3R,4S,5S,6R)-3,4,5-trihydroxy-6-(hydroxymethyl)oxan-2-yl]oxynaphthalen-2-yl]ethanone, and oleic acid. Prominent downregulated metabolites included excavatin M, perindopril, (±)-alpha-lipoic acid amide, cynarin, and O-phosphoethanolamine (Supplementary Table S5). The functional classification analysis shows that approximately 60% of these differential metabolites belong to fatty acids and conjugates, steroids, amino acids and peptides, isoprenoids, or steroids. KEGG analysis revealed their predominant involvement in: phenylalanine metabolism, citrate cycle (TCA cycle), alanine/aspartate/glutamate metabolism, phenylalanine/tyrosine/tryptophan biosynthesis, biosynthesis of unsaturated fatty acids, tyrosine metabolism, ascorbate and aldarate metabolism, primary bile acid biosynthesis, arginine biosynthesis, and butanoate metabolism (Figure 3B).

The CADOSA versus CAD analysis yielded 252 differential metabolites (154 upregulated, 98 downregulated, adjusted $p<0.05$). The top upregulated metabolites were tryptophan, 1-[8-hydroxy-3-methyl-1-[(2S,3R,4S,5S,6R)-3,4,5-trihydroxy-6-(hydroxymethyl)oxan-2-yl]oxynaphthalen-2-yl]ethanone, tebufenozide, deferasirox, and oleic acid, while the most significantly downregulated metabolites included indolelactic acid, 1234_tetrahydro_beta_carboline_carboxylic_acid, LPE 16:0, PI 34:2, and 5-hydroxy-2,2-dimethyl-7,10-bis(2-methylbut-3-en-2-yl)pyrano[3,2-g]chromen-8-one (Supplementary Table S6). These metabolites were predominantly (56%) classified as fatty acids and conjugates, amino acids and peptides, steroids, sterols, or benzoic acids. The top enriched pathways included: valine/leucine/isoleucine biosynthesis, biosynthesis of unsaturated fatty acids, phenylalanine/tyrosine/tryptophan biosynthesis, valine/leucine/isoleucine degradation, tyrosine metabolism, primary bile acid biosynthesis, aminoacyl-tRNA biosynthesis, phenylalanine metabolism, alpha-linolenic acid metabolism, and arginine biosynthesis (Figure 3C). Venn diagram analysis of pathway enrichment across all three comparisons identified two common pathways: biosynthesis of unsaturated fatty acids and phenylalanine metabolism. However, phenylalanine metabolism was also implicated in the metabolic pathways associated with differentially expressed genes in OSA (Figures 2C and 3D).

Screening of Specific Diagnostic Markers Among Three Disease Conditions

Based on the pairwise comparison data of OSA vs HC and CAD vs HC, a Venn diagram was generated to identify common differentially expressed metabolites (Figure 4A). The results revealed 144 non-overlapping metabolites as unique differential metabolites in OSA and 54 in CAD, among which 41 were endogenous metabolites in the OSA group and 25 in the CAD group (Supplementary Table S7). Furthermore, the three-group comparisons of CADOSA vs HC, CADOSA vs OSA, and CADOSA vs CAD identified 29 common differential metabolites with 15 being endogenous metabolites (Supplementary Table S8), of which showed no overlap with the OSA or CAD specific metabolites, supporting their potential as candidate metabolic biomarkers for the individual diseases (OSA and CAD) and their comorbidity (Figure 4B).

Based on the screened disease-specific endogenous metabolites for OSA, CAD, and CADOSA, we employed three multivariate discriminant models Elastic Net Regression, Random Forest, and linear SVM to establish diagnostic models and identify predictive metabolic biomarkers for each disease. Using the top five disease-specific metabolites for OSA, CAD, and CADOSA, we constructed diagnostic models and evaluated the AUC of each individual metabolite.

For OSA, the results demonstrated that the top five metabolites effectively distinguished samples from the disease and healthy controls in PCA clustering analysis (Figure 5A). All three machine learning models achieved a prognostic AUC of 1, indicating robust diagnostic accuracy (Figure 5B). ROC curve analysis of individual key metabolites revealed that

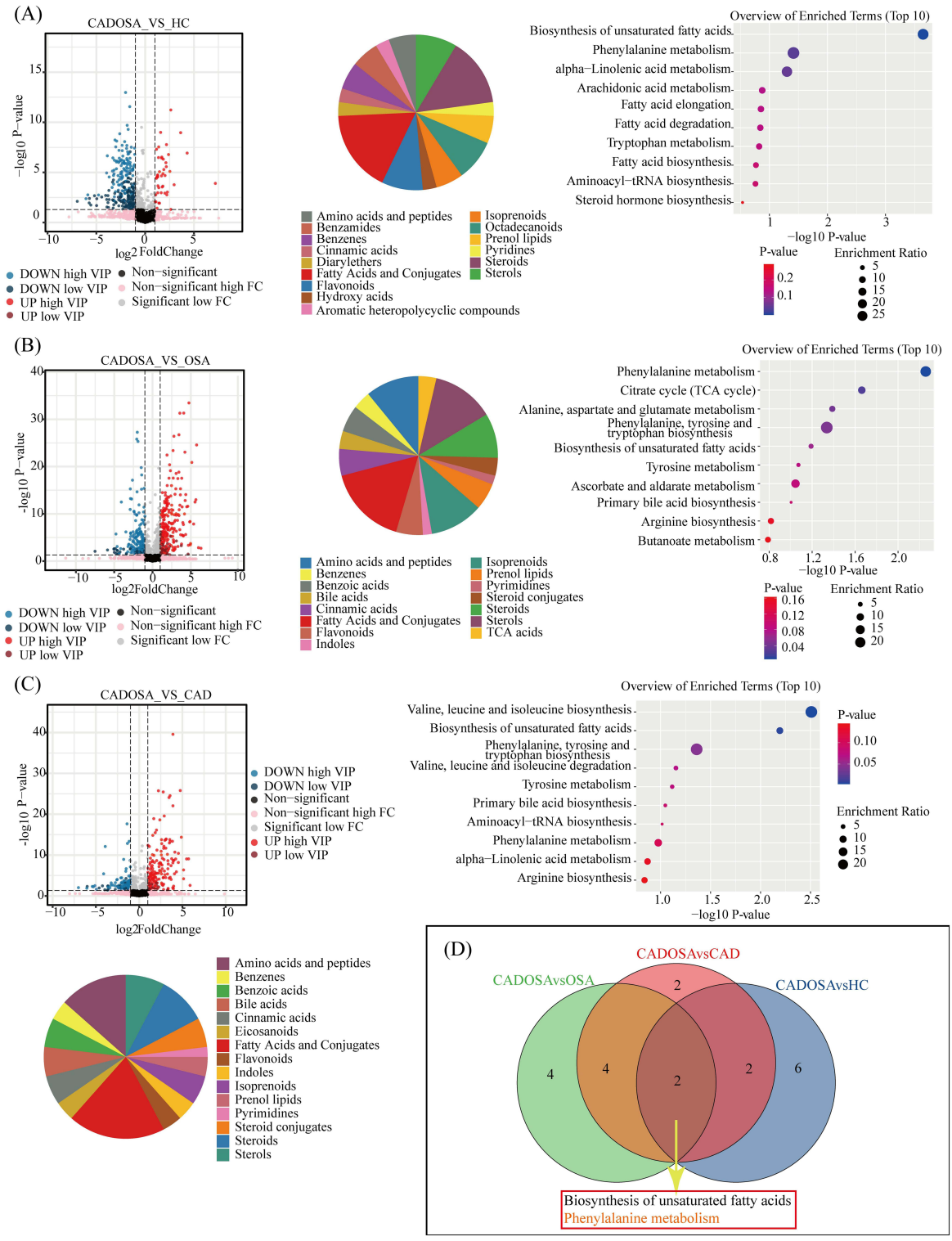

Figure 3 Differential metabolite analysis of the CADOSA group. (**A**) Volcano plot displays the differential metabolite expression levels between CADOSA and HC. Green dots represent downregulated differentially expressed metabolites, while red dots indicate upregulated ones. The pie chart illustrates the functional classification of differential metabolites. The bubble plot shows the top 10 KEGG pathways enriched by differential metabolites. (**B**) Volcano plot presents the differential metabolite expression levels between CADOSA and OSA. Green dots denote downregulated differentially expressed metabolites, whereas red dots signify upregulated ones. The pie chart depicts the functional classification of differential metabolites. The bubble plot displays the top 10 KEGG pathways enriched by differential metabolites. (**C**) Volcano plot illustrates the differential metabolite expression levels between CADOSA and CAD. Green dots indicate downregulated differentially expressed metabolites, while red dots represent upregulated ones. The pie chart demonstrates the functional classification of differential metabolites. The bubble plot exhibits the top 10 KEGG pathways enriched by differential metabolites. (**D**) Venn diagram reveals the overlapping and group-specific pathways among the three comparisons: CADOSA vs HC, CADOSA vs OSA, and CADOSA vs CAD.

https://doi.org/10.2147/NSS.S575902

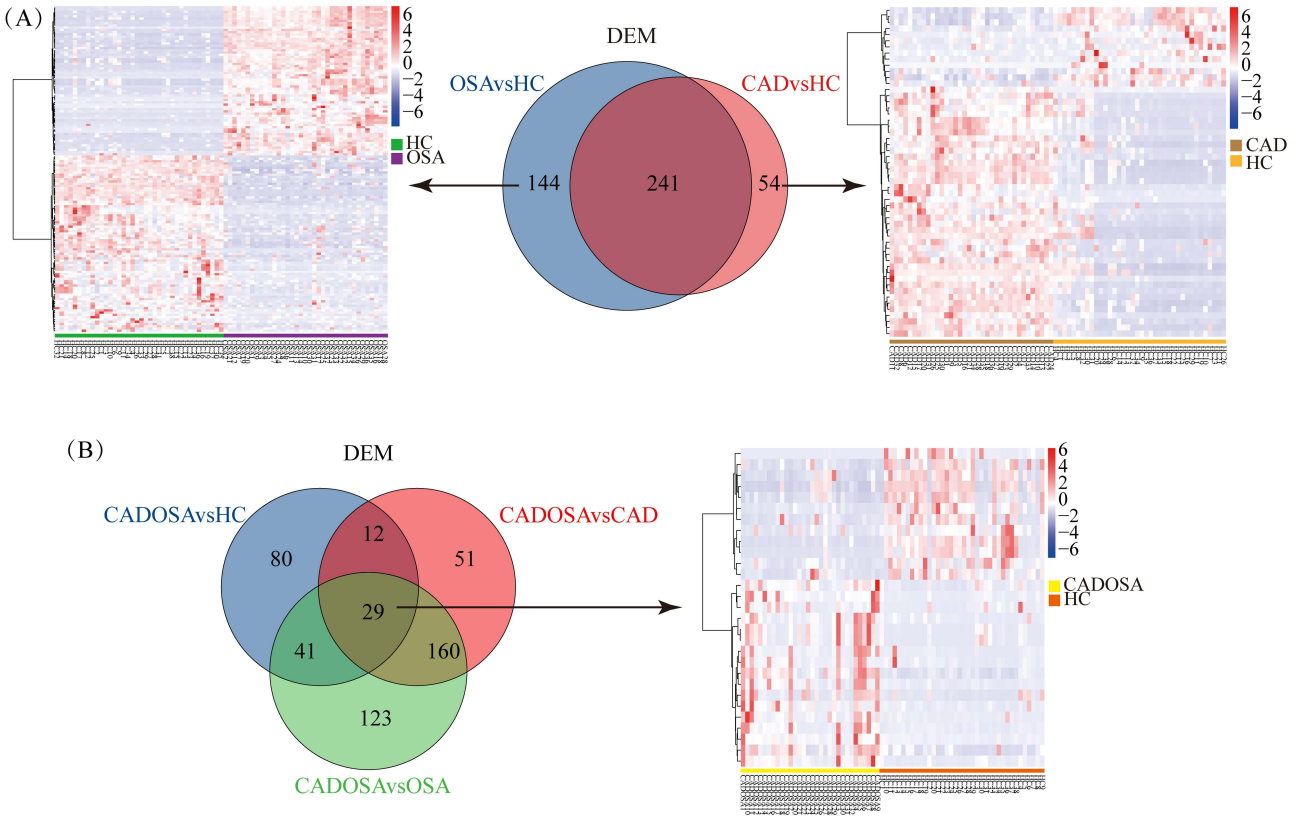

Figure 4 Screening of specific metabolic biomarkers. (**A**) Venn diagram displaying overlapping and group-specific metabolites between OSA vs HC and CAD vs HC, with arrows indicating the expression heatmap of specific DEMs. (**B**) Venn diagram illustrating overlapping and group-specific metabolites among CADOSA vs HC, CADOSA vs OSA, and CADOSA vs CAD, with arrows pointing to the expression heatmap of specific DEMs.

the elevated D-glucuronolactone (OSA-M2) in OSA patients as exhibiting the highest diagnostic performance, with an AUC of 0.996, a sensitivity of 0.947, and a specificity of 1. Succinate (OSA-M1), (R)-4-((3R,5R,8R,9S,10S,12S,13R,14S,17R)-3,12-dihydroxy-10,13-dimethylhexadecahydro-1H-cyclopenta[a]phenanthren-17-yl)-N-(pyridin-2-ylmethyl)pentanamide (OSA-M3), dyphylline (OSA-M4), and (5S)-17-hydroxy-10,13-dimethyltetradecahydro-1H-cyclopenta[a]phenanthren-3(2H)-one (OSA-M5) also showed high AUC values of 0.993, 0.994, 1.000, and 0.977, respectively (Figure 5C and D). Correlation analysis indicated that OSA-M2, the metabolite with the highest diagnostic performance and expression level, was positively correlated with OSA-M1, OSA-M4, and OSA-M5 but negatively correlated with OSA-M3 (Figure 5E).

In CAD, sample clustering based on the top5 metabolites also effectively distinguished in two groups (Figure 6A). The random forest and SVM-based OSA models exhibited same robust diagnostic accuracy (AUC=0.973, Figure 6B). ROC curve analysis of each key metabolite revealed that elevated 12-hydroxyoctadecanoic acid (CAD-M1) had an AUC value of 0.91, a sensitivity of 0.842, and a specificity of 0.944. 12-HEPE (CAD-M2), 17-hydroxyprogesterone (CAD-M3), thymidine-5-diphosphate sodium salt (CAD-M4), and psilocybin (CAD-M5) showed AUC values of 0.882, 0.791, 0.88, and 0.825, respectively (Figure 6C and D). Correlation analysis further demonstrated that CAD-M1was positively correlated with CAD-M2, M3, M4, and M5 (Figure 6E).

For CADOSA, the top5 metabolites-based PCA also displayed an effective distinguishing in samples from CADOSA and HC groups (Figure 7A). The elastic net and SVM-based OSA models exhibited robust diagnostic accuracy (AUC=0.889) (Figure 7B). ROC curve analysis of individual key metabolites revealed that the significant downregulation of tryptophan achieved an AUC of 0.972, with a sensitivity of 0.868, and a specificity of 0.969. [6]-shogaol, C12-AE1S, bufalin, and IBMX showed AUC values of 0.954, 0.905, 0.888, and 0.831, respectively (Figure 7C and D).

 https://doi.org/10.2147/NSS.S575902

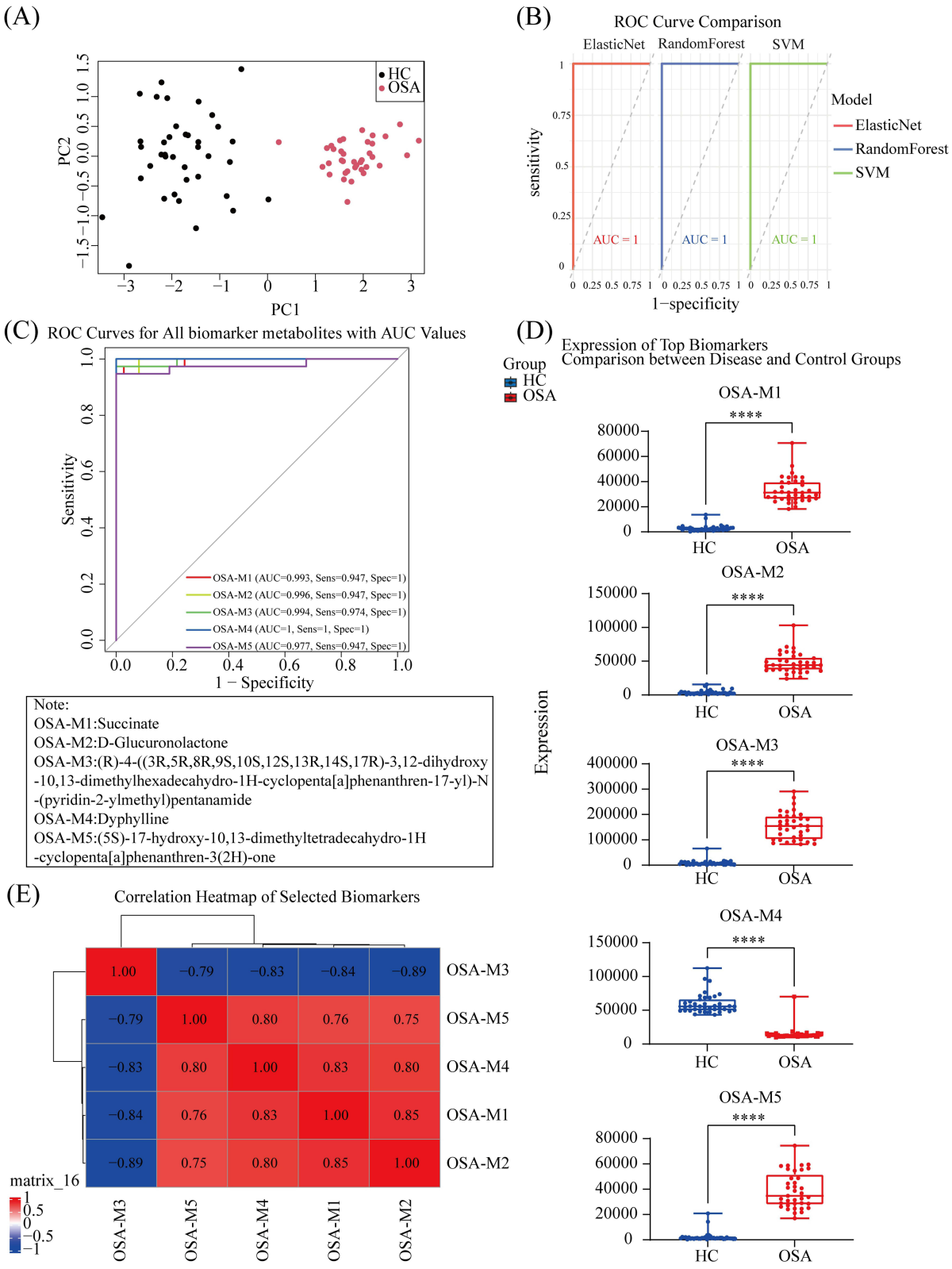

Figure 5 OSA diagnostic model construction and metabolic biomarkers screening. (**A**) PCA revealed that specific metabolites showed high cohesion and good separation between the OSA group (in pink) and the HC group (in black). (**B**) Compare the AUC values of the Elastic Net Regression, Random Forest, and linear SVM model. (**C**) ROC curves for metabolic biomarkers. (**D**) Correlation heatmap of OSA biomarkers. (**E**) Comparison of the expression of biomarkers between the OSA and HC groups. (**** $p<0.0001$).

https://doi.org/10.2147/NSS.S575902

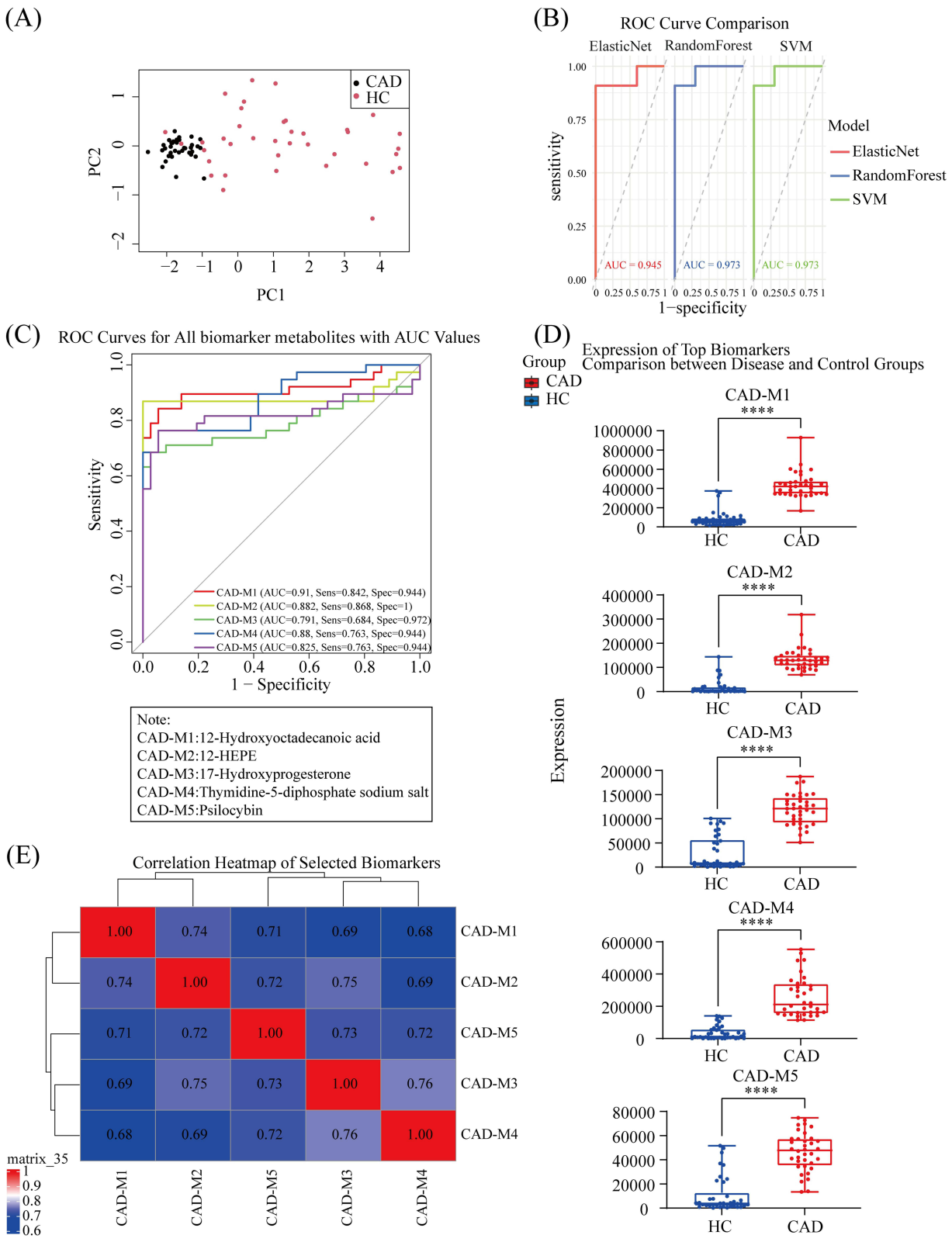

Figure 6 CAD diagnostic model construction and metabolic biomarkers screening. (**A**) PCA revealed that specific metabolites showed high cohesion and good separation between the CAD group (in black) and the HC group (in pink). (**B**) Compare the AUC values of the Elastic Net Regression, Random Forest, and linear SVM model. (**C**) ROC curves for metabolic biomarkers. (**D**) Correlation heatmap of CAD biomarkers. (**E**) Comparison of the expression of biomarkers between the CAD and HC groups. (**** p<0.0001).

https://doi.org/10.2147/NSS.S575902

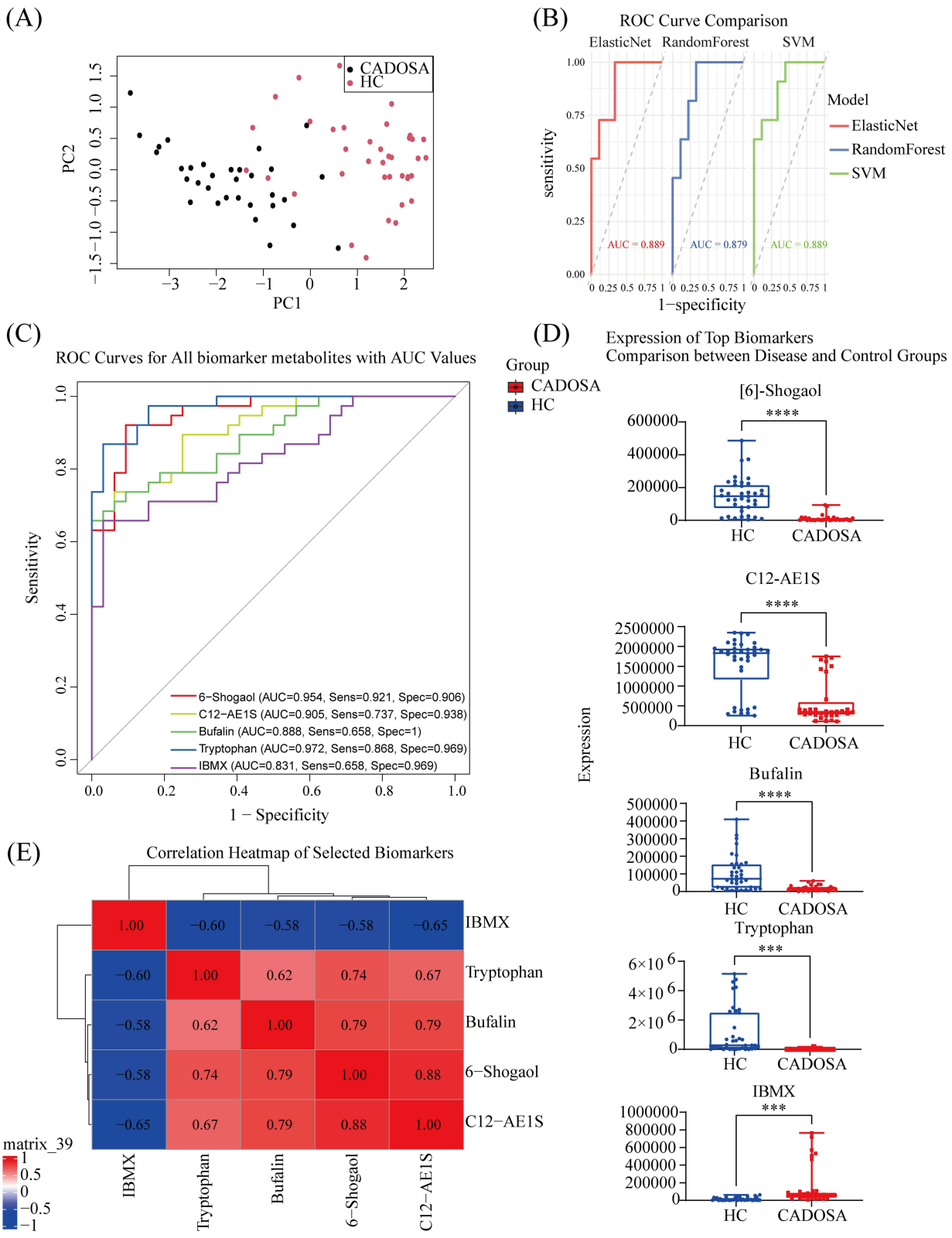

Figure 7 CADOSA diagnostic model construction and metabolic biomarkers screening. (**A**) PCA revealed that specific metabolites showed high cohesion and good separation between the CADOSA group (in black) and the HC group (in pink). (**B**) Compare the AUC values of the Elastic Net Regression, Random Forest, and linear SVM model. (**C**) ROC curves for metabolic biomarkers. (**D**) Correlation heatmap of CADOSA biomarkers. (**E**) Comparison of the expression of biomarkers between the CADOSA and HC groups. (** p<0.01,**** p<0.0001).

https://doi.org/10.2147/NSS.S575902

Correlation analysis demonstrated that tryptophan was positively correlated with [6]-shogaol, C12-AE1S, and bufalin, but negatively correlated with IBMX (Figure 7E).

Correlation Network Between Differential Expressed Metabolites and Transcriptomic Genes in CADOSA

To investigate the potential regulatory mechanisms of CADOSA-related metabolic molecules, we performed correlation analyses between CADOSA five endogenous metabolic marker molecules and gene expression from paired transcriptomic data.[11]

The interaction network revealed significant correlations ($|R| \geq 0.7$, $p<0.05$) between CADOSA top 5 differential metabolites and 376 differentially expressed genes (DEGs) in the CADOSA vs HC comparison. We found that the most highly expressed and upregulated metabolite IBMX showed strong positive correlations with the highly expressed genes FCAR, PLBD1, and BPI. The downregulated metabolite C12-AE1S exhibited significant positive correlations with ZDHHC11B, TENT5C, and SPMIP8. The downregulated bufalin strongly correlated to GSTM3, CA6, and RBM11. The downregulated tryptophan exhibited strong positive correlations with DMXL2, CCDC88A, and TIMD4. The decreased metabolite 6-shogaol was correlated significantly with GPR15, GAGE10, and LILRB5 (Figure 8A).

Functional enrichment analysis indicated that the top 5 metabolites highly interacting genes are predominantly enriched in pathways of ECM−receptor interaction, proteoglycans in cancer, human papillomavirus infection, cytoskeleton in muscle cells, NOD−like receptor signaling pathway, melanogenesis, amoebiasis, protein digestion and absorption, transcriptional mis-regulation in cancer, and focal adhesion (Figure 8B).

Discussion

OSA characterized by recurrent upper airway collapse during sleep, is an established independent risk factor for CAD.[29] CAD develops from coronary atherosclerosis, leading to luminal stenosis, myocardial ischemia, and necrosis. These conditions mutually exacerbate each other through shared mechanisms such as oxidative stress, endothelial dysfunction, and metabolic dysregulation, forming a vicious cycle that worsens prognosis. Despite rising clinical prevalence of CAD and OSA comorbidity (CADOSA),[30] research has largely focused on isolated diseases, leaving its metabolomic signatures and diagnostic implications poorly understood. Given the importance of biomarkers in risk stratification and early intervention, we conducted a comprehensive metabolomic analysis comparing OSA, CAD, and CADOSA patients with healthy controls. Our study aimed to identify distinct metabolic patterns in comorbid patients versus those with single diseases, and explore associations between key metabolites and gene regulatory networks to uncover underlying mechanisms.

Clinically, the OSA group showed significantly elevated DBP and RBC counts, whereas the CAD group exhibited increased NT-proBNP levels, reflecting heightened myocardial injury risk. Notably, CADOSA patients displayed pronounced abnormalities in left ventricular dimensions (LVD, LVS), AHI, and SpO_2, indicating exacerbated cardiac dysfunction and sleep-disordered breathing severity, consistent with echocardiographic and PSG findings. However, contrary to prior research,[31] DBP and RBC levels were significantly higher in the OSA group than in the CADOSA group, possibly due to pre-admission pharmacological interventions in comorbid patients.

Our analysis revealed significant metabolic commonalities between CAD and OSA. Both the differential metabolite profiling and KEGG enrichment analysis demonstrated that these two conditions are primarily associated with dysregulation in fatty acid, steroid, amino acid, and energy metabolism pathways, including biosynthesis of unsaturated fatty acids, steroid hormone biosynthesis, citrate cycle (TCA cycle), alanine, aspartate and glutamate metabolism, tyrosine metabolism, and fatty acid biosynthesis, among others. These findings are highly consistent with previous reports,[32–36] further substantiating the crucial role of these metabolic pathways in disease pathogenesis.

Our study revealed distinct metabolic disturbances in OSA, particularly affecting ascorbate and aldarate metabolism, alpha-linolenic acid (ALA) metabolism, and primary bile acid biosynthesis. Although ascorbate and aldarate metabolism has not been previously linked to OSA, its known antioxidant properties including mitochondrial stabilization and nitric oxide-mediated vasodilation,[37,38] suggest that IH-induced ROS and HIF-1α accumulation may disrupt this pathway,

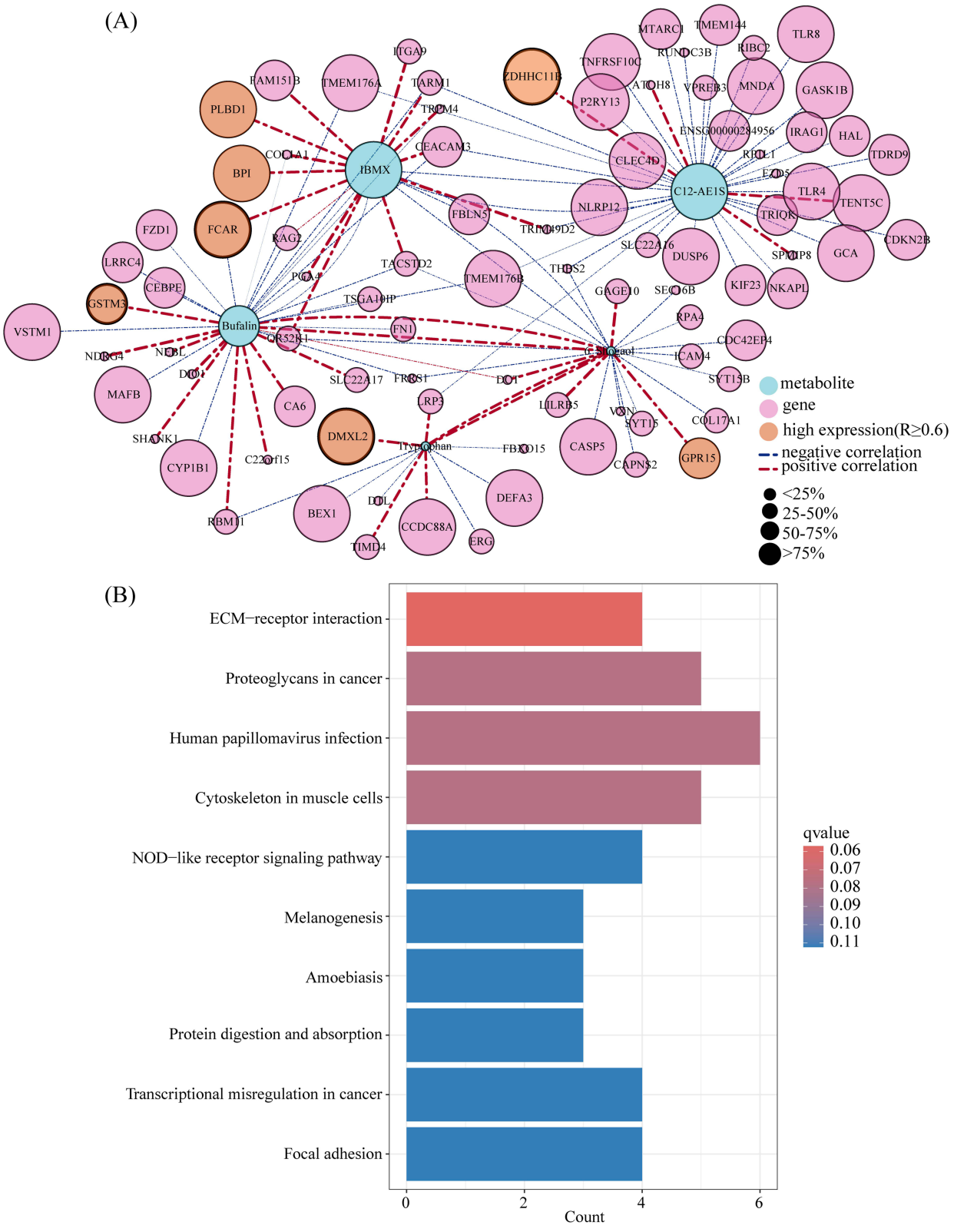

Figure 8 Association analysis of transcriptome and metabolome in CADOSA. (**A**) Interaction network between genes and five key CADOSA metabolites. In the interaction graph, pink dots represent genes, blue dots represent metabolites, and Orange dots represent genes with a strong positive correlation with the metabolites. The larger the dot, the higher the expression level of the metabolite or gene. Blue lines represent the negative correlation between the two substances, while red lines represent the positive correlation. Thick segments indicate a correlation coefficient R>0.6, and thin segments indicate a correlation coefficient R of 0.4–0.6. (**B**) Pathway results of the top 5 genes interacting with metabolites.

https://doi.org/10.2147/NSS.S575902

exacerbating oxidative stress. Similarly, ALA and its derivatives (EPA/DHA) regulate inflammation, endothelial function, and lipid metabolism.[39,40] IH may impair ALA processing through cytokine release and altered enzymatic activity,[41] potentially explaining the dyslipidemia common in OSA. While primary bile acid biosynthesis has not been directly associated with OSA, HIF-1α elevated in OSA modulates this pathway in non-alcoholic fatty liver disease (NAFLD).[42] Mechanistically, IH may further dysregulate bile acids via gut microbiota disruption,[43] worsening metabolic and cardiovascular sequelae.[44] Collectively, HIF-1α activation and inflammatory signaling likely drive these metabolic perturbations, accelerating OSA progression. Notably, machine learning identified D-glucuronolactone as the top OSA-specific biomarker, supported by its high AUC and differential expression.

Our study identified distinct CAD-associated metabolic perturbations in arginine biosynthesis, sphingolipid metabolism, pyruvate metabolism, and glycerophospholipid metabolism. Arginine, a NO precursor, is critical for vascular endothelial function and platelet inhibition.[45] Its dysregulation in CAD patients correlates with endothelial dysfunction, consistent with clinical evidence that shows L-arginine supplementation improves endothelial function and reduces LDL oxidation.[46] Sphingolipid metabolism also plays a key role in CAD pathogenesis, primarily through ceramides and sphingosine-1-phosphate (S1P). Elevated ceramides, established biomarkers for CAD, promote disease progression via lipid deposition and impaired NO signaling,[47,48] while S1P dysregulation exacerbates endothelial instability and inflammation.[49,50] Altered pyruvate metabolism reflects myocardial metabolic reprogramming in CAD. Ischemia-hypoxia shifts energy production toward anaerobic glycolysis, reducing TCA cycle activity and increasing lactate accumulation. This impairs ATP generation, exacerbates cardiomyocyte apoptosis, and may activate NLRP3 inflammasome mediated injury.[51,52] Pyruvate metabolism disruptions may further worsen CAD by dysregulating lipid metabolism, accelerating cholesterol/triglyceride deposition.[53–55] Aberrant glycerophospholipid metabolism aligns with prior findings,[56] where its dysregulation impairs endothelial function, pro-inflammatory activation, and dyslipidemia.[57] Notably, phosphatidylthreonine (PT) and related glycerophospholipids correlate strongly with CAD severity,[58] highlighting their potential as diagnostic or therapeutic targets. These findings corroborate existing literature, validating our methodological approach. These findings validate established CAD mechanisms while introducing 12-hydroxyoctadecanoic acid as a novel endogenous biomarker, supported by its optimal AUC and differential expression.

The identification of early diagnostic biomarkers for CAD-OSA comorbidity was a key focus of this study. Metabolomic profiling revealed that CADOSA-associated differential metabolites primarily fell into four categories: fatty acids/conjugates, steroids/sterols, and amino acids/peptides. Of these, unsaturated fatty acid biosynthesis exhibited dual regulatory potential. Although some evidence suggests polyunsaturated fatty acids (PUFAs) may reduce CAD incidence and mortality.[59,60] Mendelian randomization analyses[5,49] and clinical trials[61] have yielded inconsistent evidence to support these benefits. Conversely, omega-3 supplementation may improve OSA by mitigating inflammation, insulin resistance, and dyslipidemia.[62] Phenylalanine metabolism has emerged as another critical pathway, influencing mitochondrial function and hypoxia adaptation via hepatocyte energy metabolism and macrophage cytokine regulation.[63–65] We hypothesize that intermittent hypoxia-induced oxidative stress may disrupt this pathway, leading to phenylalanine derivative accumulation (eg, phenylacetate). These metabolites could exacerbate endothelial dysfunction, neurotoxicity, and atherosclerosis,[66] thereby elevating the overall risk for CAD. Among CADOSA-specific metabolites, tryptophan showed superior diagnostic performance (AUC and expression levels), positioning it as a promising biomarker for this comorbidity.

To explore the molecular mechanisms of CADOSA, we integrated multi-omics data with prior transcriptomic findings,[11] identifying five CADOSA-specific metabolite-gene networks. Notably, the differential metabolite C12-AE1S formed a robust interaction module with ZDHHC11B, a gene linked to lipid metabolism and inflammation. ZDHHC11B, an endoplasmic reticulum protein, inhibits fatty acid mobilization by suppressing lipophagy and lipolysis in lipid droplets.[67] It also activates the STING-NF-κB pathway, driving type I interferon and proinflammatory cytokine production.[68–71] In cancer, ZDHHC11B promotes tumor progression via palmitoylation of EMT-related molecules. We hypothesize that in CADOSA, ZDHHC11B may exacerbate airway collapse and hypoxia by inducing EMT, leading to airway remodeling, fibrosis, and vascular endothelial dysfunction. This could accelerate atherosclerotic plaque vulnerability and vascular injury. Our findings suggest that ZDHHC11B upregulation in CADOSA may bridge C12-AE1S

mediated lipid dysregulation and EMT-driven pathogenesis. Future studies using OSA-atherosclerosis animal models are needed to validate whether ZDHHC11B contributes to disease progression via C12-AE1S dependent mechanisms.

The strong IBMX-FCAR correlation suggests a potential regulatory interaction in CADOSA. IBMX, a non-specific phosphodiesterase (PDE) inhibitor, increases cAMP/PKA activity, which may worsen tachycardia, blood pressure instability,[72–74] enhancing insulin secretion,[75] and increasing myocardial sensitivity to hypoxia.[76] Conversely, FCAR (CD89), primarily expressed in myeloid cells (eg, neutrophils, macrophages),[77,78] promotes thrombosis via neutrophil extracellular trap (NET) activation.[78] and intermittent hypoxia (IH) in OSA may amplify FCAR-mediated inflammation, exacerbating endothelial injury.[77] Notably, FCAR polymorphisms (eg, Asp92Asn) are linked to cardiovascular risk in males,[79] while FCAR inhibition attenuates ox-LDL–driven foam cell formation, MAPK signaling, and proinflammatory cytokines, thereby slowing atherosclerosis.[80,81] We propose that IBMX upregulation in CADOSA may enhance myocardial hypoxia susceptibility and FCAR activation, aggravating cardiac inflammation. Additionally, IBMX-induced increased myocardial contractility could elevate coronary mechanical stress. Under hypoxia, these mechanisms may synergistically accelerate CAD progression.

In CADOSA patients, tryptophan was the only significantly downregulated metabolite, consistent with prior reports in CAD and OSA.[18,82] Its levels strongly correlated with DMXL2 expression. Tryptophan metabolism occurs via three key pathways: kynurenine production, serotonin (5-HT) synthesis, and gut microbiota-dependent indole formation. IH promotes tryptophan-to-kynurenine conversion—a process heightened nocturnally,[83] which aligns with elevated kynurenine/tryptophan ratios in CAD severity.[82,84] IH also reduces 5-HT, potentially exacerbating depression-like behaviors and activating a stress-driven kynurenine pathway, perpetuating a cycle of inflammation and psychological stress that may worsen hypertension and plaque instability.[85–87] Furthermore, IH disrupts gut microbiota, impairing tryptophan absorption and indole derivative synthesis (eg, indole-3-propionic acid, IPA), which may aggravate metabolic dysfunction and inflammation.[18] IPA demonstrates cardiovascular protection by enhancing reverse cholesterol transport,[88,89] thus, IH-induced microbiota shifts could accelerate CAD progression by depleting IPA. Although DMXL2 (Rabconnectin-3) remains understudied in OSA and CAD, emerging evidence implicates it in their pathogenesis. As a key regulator of synaptic vesicle trafficking, DMXL2 modulates neuroendocrine signaling.[90] In the central nervous system, 5-HT release depends on vesicular transport, prompting our hypothesis that DMXL2 may influence 5-HT bioavailability and plaque stability. Moreover, DMXL2 promotes epithelial mesenchymal transition (EMT) via Notch pathway activation.[91,92] Given that IH stabilizes HIF-1α a known Notch pathway inducer a synergistic interaction may exacerbate upper airway and vascular remodeling in CADOSA. Collectively, we propose that DMXL2 dysregulation contributes to CADOSA progression via dual mechanisms:disrupting vesicular transport of tryptophan metabolites and inducing EMT-mediated vascular dysfunction.

This study has certain limitations. This study has several limitations. First, our cohort was predominantly male, particularly within the patient groups; therefore, the generalizability of the identified metabolomic signatures and biomarkers to females remains uncertain. Second, as a cross-sectional analysis, the present design does not permit causal inference but only reveals associations between variables. Third, potential confounding factors—such as body mass index and medication use, may have influenced the metabolomic profiles. Finally, due to time and resource constraints, external validation in an independent cohort was not performed in this phase. Future longitudinal or interventional studies are needed to establish the mechanistic roles of these metabolites in disease pathogenesis and progression. Subsequent investigations involving larger, multi-center cohorts will be essential to enhance the generalizability and robustness of our findings. If validated, the newly identified biomarkers could potentially be incorporated into existing risk stratification models. Such integration would aid in the early diagnosis and individualized risk prediction of comorbid CAD and OSA by quantifying an individual's probability of comorbidity.

Conclusions

This study elucidates the distinct plasma metabolic profiles of patients with OSA, CAD, and their comorbidity, CADOSA—a notably understudied clinical phenotype. We newly discovered D-glucuronolactone as a potential metabolic biomarker for OSA and 12-hydroxyoctadecanoic acid as a candidate biomarker for CAD. Notably, tryptophan emerges as a promising biomarker for early risk prediction in CADOSA patients. Multi-omics integration highlights biologically

plausible pathways unique to the comorbid condition. Furthermore, our analysis reveals three highly correlated metabolite-gene pairs with potential therapeutic implications for CADOSA: tryptophan-DMXL2(C12-AE1S)-ZDHHC11, and IBMX-FCAR. It should be emphasized that all associations, including those between metabolites and genes, are associative and do not imply causality. These molecules may represent novel therapeutic targets for CADOSA intervention.

Data Sharing Statement

Data generated during this study is included in this article. Further data can be accessed on request from the corresponding author.

Ethics Approval and Consent to Participate

The present study was conducted in strict accordance with the Declaration of Helsinki and its later amendments or comparable ethical standards. Our research project was approved by the Second Affiliated Hospital of Fujian Medical University (protocol code 597 and date 2023 of approval). All participants in this study provided written informed consent.

Acknowledgment

The author received assistance in the non-targeted metabolomics data analysis for this research from Hangzhou Cosmos Wisdom Company.

Author Contributions

The current statement that all authors gave final approval of the version to be published; have agreed on the journal to which the article has been submitted; and agree to be accountable for all aspects of the work. Conceptualization, Liying Yu, Shuhan Chen, and Qingquan Liu; Investigation, Liying Yu, Shuhan Chen, and Wanqi Li; Methodology, Liying Yu, Shuhan Chen, and Jing Liu; Resources, Qingquan Liu and Liying Yu; Supervision, Liying Yu; Validation, Shuhan Chen, Jing Liu, and Huijuan Zheng; Writing – original draft, Shuhan Chen Qingquan Liu, Jing Liu, Huijuan Zheng, Wanqi Li and Liying Yu; Writing – review & editing, Liying Yu and Qingquan Liu.

Funding

This study was supported by the Joint funds for the innovation of science and technology, Fujian province (Grant number: 2023Y9261), Quanzhou High-level Talent Introduction Program (2023CT014), Fujian Provincial Joint Funds for Science and Technology Innovation (2024Y9401).

Disclosure

The authors declare that they have no competing interests in this study.

References

1. Wang X, Fan J, Guo R, et al. Association of obstructive sleep apnoea with cardiovascular events in women and men with acute coronary syndrome. *Eur Respir J*. 2023;61(1):2201110. doi:10.1183/13993003.01110-2022
2. Piepoli MF, Hoes AW, Agewall S, et al. 2016 European guidelines on cardiovascular disease prevention in clinical practice. *Rev Esp Cardiol*. 2016;69(10):939. doi:10.1016/j.rec.2016.09.009
3. Center For Cardiovascular Diseases The Writing Committee Of The Report On Cardiovascular Health And Diseases In China N; Center For Cardiovascular Diseases The Writing Committee Of The Report On Cardiovascular H, Diseases In China N. Report on cardiovascular health and diseases in China 2023: an updated summary. *Biomed Environ Sci*. 2024;37(9):949–992. doi:10.3967/bes2024.162
4. Suen C, Wong J, Ryan CM, et al. Prevalence of undiagnosed obstructive sleep apnea among patients hospitalized for cardiovascular disease and associated in-hospital outcomes: a scoping review. *J Clin Med*. 2020;9(4):989. doi:10.3390/jcm9040989
5. Chang JL, Goldberg AN, Alt JA, et al. International consensus statement on obstructive sleep apnea. *Int Forum Allergy Rhinol*. 2023;13(7):1061–1482.
6. Heraganahally SS, Rajaratnam B, Silva S, et al. Obstructive sleep apnoea and cardiac disease among aboriginal patients in the Northern Territory of Australia. *Heart Lung Circ*. 2021;30(8):1184–1192. doi:10.1016/j.hlc.2021.01.007

7. Li Y, Miao Y, Zhang Q. Causal associations of obstructive sleep apnea with cardiovascular disease: a Mendelian randomization study. *Sleep*. 2023;46(3). doi:10.1093/sleep/zsac298
8. Yeghiazarians Y, Jneid H, Tietjens JR, et al. Obstructive sleep apnea and cardiovascular disease: a scientific statement from the American Heart Association. *Circulation*. 2021;144(3):e56–e67. doi:10.1161/CIR.0000000000000988
9. Sánchez-de-la-Torre M, Sánchez-de-la-Torre A, Bertran S, et al. Effect of obstructive sleep apnoea and its treatment with continuous positive airway pressure on the prevalence of cardiovascular events in patients with acute coronary syndrome (ISAACC study): a randomised controlled trial. *Lancet Respir Med*. 2020;8(4):359–367. doi:10.1016/S2213-2600(19)30271-1
10. Chen R, Quan J, Tang Q, et al. Association between NoSAS score and cardiovascular disease in patients with obstructive sleep apnea. *Front Cardiovasc Med*. 2025;12:1572055
11. Liu Q, Chen X, Chen S, et al. Integrative transcriptomic analysis reveals diagnostic biomarkers for comorbidity of coronary artery disease and obstructive sleep apnea. *Front Cardiovasc Med*. 2025;12:1658016
12. Li C, Shi S. Gut microbiota and metabolic profiles in chronic intermittent hypoxia-induced rats: disease-associated dysbiosis and metabolic disturbances. *Front Endocrinol*. 2023;14:1224396. doi:10.3389/fendo.2023.1224396
13. Zhang D, Wang Q, Li D, et al. Gut microbiome composition and metabolic activity in metabolic-associated fatty liver disease. *Virulence*. 2025;16 (1):2482158. doi:10.1080/21505594.2025.2482158
14. Brito Rodrigues P, de Rezende Rodovalho V, Sencio V, et al. Integrative metagenomics and metabolomics reveal age-associated gut microbiota and metabolite alterations in a hamster model of COVID-19. *Gut Microbes*. 2025;17(1):2486511. doi:10.1080/19490976.2025.2486511
15. Xue J, Allaband C, Zuffa S, et al. Gut microbiota and derived metabolites mediate obstructive sleep apnea induced atherosclerosis. *Gut Microbes*. 2025;17(1):2474142. doi:10.1080/19490976.2025.2474142
16. Castillo-Peinado LS, Calderón-Santiago M, Jurado-Gámez B, et al. Changes in human sweat metabolome conditioned by severity of obstructive sleep apnea and intermittent hypoxemia. *J Sleep Res*. 2024;33(4):e14075. doi:10.1111/jsr.14075
17. Wang X, Zhao J, Wang X, et al. Metabolomic profiles predict clinical severity in patients with obstructive sleep apnea-hypopnea syndrome. *J Clin Sleep Med*. 2024;20(9):1445–1453. doi:10.5664/jcsm.11160
18. Wang F, Zou J, Xu H, et al. Effects of chronic intermittent hypoxia and chronic sleep fragmentation on gut microbiome, serum metabolome, liver and adipose tissue morphology. *Front Endocrinol*. 2022;13:820939. doi:10.3389/fendo.2022.820939
19. Zhang X, Wang S, Xu H, et al. Metabolomics and microbiome profiling as biomarkers in obstructive sleep apnoea: a comprehensive review. *Eur Respir Rev*. 2021;30(160):200220. doi:10.1183/16000617.0220-2020
20. Zhang Y, Ngo D, Yu B, et al. Development and validation of a metabolite index for obstructive sleep apnea across race/ethnicities. *Sci Rep*. 2022;12 (1):21805. doi:10.1038/s41598-022-26321-9
21. Wang TJ. Assessing the role of circulating, genetic, and imaging biomarkers in cardiovascular risk prediction. *Circulation*. 2011;123(5):551–565. doi:10.1161/CIRCULATIONAHA.109.912568
22. Fan Y, Li Y, Chen Y, et al. Comprehensive metabolomic characterization of coronary artery diseases. *J Am Coll Cardiol*. 2016;68(12):1281–1293. doi:10.1016/j.jacc.2016.06.044
23. Kondraciuk M, Chlabicz M, Jamiołkowski J, et al. Coronary artery disease is associated with particular change of serum metabolome: a case-control study. *Metabolomics*. 2025;21(3):57. doi:10.1007/s11306-025-02253-z
24. Lai C, Li Y, Luo W, et al. Plasma metabolomics differentiating and predicting prognosis of coronary artery disease patients with distinct nutritional status. *Nutr Res*. 2025;137:1–13. doi:10.1016/j.nutres.2025.01.004
25. Hemmati M, Kashanipoor S, Mazaheri P, et al. Importance of gut microbiota metabolites in the development of cardiovascular diseases (CVD). *Life Sci*. 2023;329:121947. doi:10.1016/j.lfs.2023.121947
26. Wang Y, Wang X, Luo J, et al. Urinary epinephrine sulfate can predict cardiovascular risk in moderate-to-severe OSA: a metabolomics-based study. *Nat Sci Sleep*. 2024;16:1153–1168. doi:10.2147/NSS.S470154
27. Lebkuchen A, Carvalho VM, Venturini G, et al. Metabolomic and lipidomic profile in men with obstructive sleep apnoea: implications for diagnosis and biomarkers of cardiovascular risk. *Sci Rep*. 2018;8(1):11270. doi:10.1038/s41598-018-29727-6
28. Zhou EH, Zhou TJ, Wang XT, et al. Identifying and validating immunological biomarkers in obstructive sleep apnea through bioinformatics analysis. *Sci Rep*. 2025;15(1):9746. doi:10.1038/s41598-025-93915-4
29. Dong JY, Zhang YH, Qin LQ. Obstructive sleep apnea and cardiovascular risk: meta-analysis of prospective cohort studies. *Atherosclerosis*. 2013;229(2):489–495. doi:10.1016/j.atherosclerosis.2013.04.026
30. Bauters F, Rietzschel ER, Hertegonne KB, et al. The link between obstructive sleep apnea and cardiovascular disease. *Curr Atheroscler Rep*. 2016;18(1):1. doi:10.1007/s11883-015-0556-z
31. Chen Z, Han H, Liu X, et al. 阻塞性睡眠呼吸暂停综合征和高血压关系的研究进展 [The Relationship Between Obstructive Sleep Apnea Syndrome and Hypertension]. *Adv Cardiovasc Dis*. 2025;46(03):193–197.
32. Savransky V, Nanayakkara A, Li J, et al. Chronic intermittent hypoxia induces atherosclerosis. *Am J Respir Crit Care Med*. 2007;175 (12):1290–1297. doi:10.1164/rccm.200612-1771OC
33. Humer E, Pieh C, Brandmayr G. Metabolomics in sleep, insomnia and sleep apnea. *Int J Mol Sci*. 2020;21(19):7244. doi:10.3390/ijms21197244
34. Xia W, Yu H, Wang G. Coronary artery disease with elevated levels of HDL cholesterol is associated with distinct lipid signatures. *Metabolites*. 2023;13(6):695. doi:10.3390/metabo13060695
35. Liao Y, Dong Z, Liao H, et al. Lipid metabolism patterns and relevant clinical and molecular features of coronary artery disease patients: an integrated bioinformatic analysis. *Lipids Health Dis*. 2022;21(1):87. doi:10.1186/s12944-022-01696-w
36. Zhong J, Wu D, Zeng Y, et al. The microbial and metabolic signatures of patients with stable coronary artery disease. *Microbiol Spectr*. 2022;10(6): e0246722. doi:10.1128/spectrum.02467-22
37. Liang H, Song K. Elucidating ascorbate and aldarate metabolism pathway characteristics via integration of untargeted metabolomics and transcriptomics of the kidney of high-fat diet-fed obese mice. *PLoS One*. 2024;19(4):e0300705. doi:10.1371/journal.pone.0300705
38. He WJ, Li C, Mi X, et al. An untargeted metabolomics study of blood pressure: findings from the Bogalusa Heart Study. *J Hypertens*. 2020;38 (7):1302–1311. doi:10.1097/HJH.0000000000002363
39. Smorenburg JN, Hodun K, McTavish PV, et al. EPA/DHA but not ALA reduces visceral adiposity and adipocyte size in high fat diet-induced obese delta-6 desaturase knockout mice. *Mol Nutr Food Res*. 2025;69(2):e202400721. doi:10.1002/mnfr.202400721

40. Wang M, Zhang XJ, Feng K, et al. Dietary α-linolenic acid-rich flaxseed oil prevents against alcoholic hepatic steatosis via ameliorating lipid homeostasis at adipose tissue-liver axis in mice. *Sci Rep*. 2016;6:26826. doi:10.1038/srep26826
41. Bruder ED, Lee PC, Raff H. Metabolomic analysis of adrenal lipids during hypoxia in the neonatal rat: implications in steroidogenesis. *Am J Physiol Endocrinol Metab*. 2004;286(5):E697–703. doi:10.1152/ajpendo.00502.2003
42. Asai Y, Yamada T, Tsukita S, et al. Activation of the hypoxia inducible factor 1α subunit pathway in steatotic liver contributes to formation of cholesterol gallstones. *Gastroenterology*. 2017;152(6):1521–35.e8. doi:10.1053/j.gastro.2017.01.001
43. Wang J, Zhu N, Su X, et al. Gut-Microbiota-Derived metabolites maintain gut and systemic immune homeostasis. *Cells*. 2023;12(5):793.
44. Staley C, Weingarden AR, Khoruts A, et al. Interaction of gut microbiota with bile acid metabolism and its influence on disease states. *Appl Microbiol Biotechnol*. 2017;101(1):47–64. doi:10.1007/s00253-016-8006-6
45. Tapiero H, Mathé G, Couvreur P, et al. I. *Arginine. Biomed Pharmacother*. 2002;56(9):439–445. doi:10.1016/S0753-3322(02)00284-6
46. Yin WH, Chen JW, Tsai C, et al. L-arginine improves endothelial function and reduces LDL oxidation in patients with stable coronary artery disease. *Clin Nutr*. 2005;24(6):988–997. doi:10.1016/j.clnu.2005.07.003
47. Poss AM, Maschek JA, Cox JE, et al. Machine learning reveals serum sphingolipids as cholesterol-independent biomarkers of coronary artery disease. *J Clin Invest*. 2020;130(3):1363–1376. doi:10.1172/JCI131838
48. Wilkerson JL, Tatum SM, Holland WL, et al. Ceramides are fuel gauges on the drive to cardiometabolic disease. *Physiol Rev*. 2024;104 (3):1061–1119. doi:10.1152/physrev.00008.2023
49. Benkhoff M, Polzin A. Lipoprotection in cardiovascular diseases. *Pharmacol Ther*. 2024;264:108747. doi:10.1016/j.pharmthera.2024.108747
50. Manzo OL, Nour J, Sasset L, et al. Rewiring endothelial sphingolipid metabolism to favor S1P over ceramide protects from coronary atherosclerosis. *Circ Res*. 2024;134(8):990–1005. doi:10.1161/CIRCRESAHA.123.323826
51. Elnwasany A, Ewida HA, Szweda PA, et al. Inhibition of pyruvate dehydrogenase in the heart as an initiating event in the development of diabetic cardiomyopathy. *Antioxidants*. 2023;12(3):756. doi:10.3390/antiox12030756
52. Ait-Aissa K, Blaszak SC, Beutner G, et al. Mitochondrial oxidative phosphorylation defect in the heart of subjects with coronary artery disease. *Sci Rep*. 2019;9(1):7623. doi:10.1038/s41598-019-43761-y
53. Du P, Guo R, Gao K, et al. Identification of differentially expressed genes and the role of PDK4 in CD14+ monocytes of coronary artery disease. *Biosci Rep*. 2021;41(4). doi:10.1042/BSR20204124
54. Panchal AR, Comte B, Huang H, et al. Acute hibernation decreases myocardial pyruvate carboxylation and citrate release. *Am J Physiol Heart Circ Physiol*. 2001;281(4):H1613–20. doi:10.1152/ajpheart.2001.281.4.H1613
55. Kumar A, Gupta P, Rana M, et al. Role of pyruvate kinase M2 in oxidized LDL-induced macrophage foam cell formation and inflammation. *J Lipid Res*. 2020;61(3):351–364. doi:10.1194/jlr.RA119000382
56. Chen H, Wang Z, Qin M, et al. Comprehensive metabolomics identified the prominent role of glycerophospholipid metabolism in coronary artery disease progression. *Front Mol Biosci*. 2021;8:632950. doi:10.3389/fmolb.2021.632950
57. Zhu Q, Wu Y, Mai J, et al. Comprehensive metabolic profiling of inflammation indicated key roles of glycerophospholipid and arginine metabolism in coronary artery disease. *Front Immunol*. 2022;13:829425. doi:10.3389/fimmu.2022.829425
58. Hajeyah AA, Protty MB, Paul D, et al. Phosphatidylthreonine is a procoagulant lipid detected in human blood and elevated in coronary artery disease. *J Lipid Res*. 2024;65(1):100484. doi:10.1016/j.jlr.2023.100484
59. Li Y, Hruby A, Bernstein AM, et al. Saturated fats compared with unsaturated fats and sources of carbohydrates in relation to risk of coronary heart disease: a prospective cohort study. *J Am Coll Cardiol*. 2015;66(14):1538–1548. doi:10.1016/j.jacc.2015.07.055
60. Zhuang P, Liu X, Li Y, et al. Circulating fatty acids, genetic risk, and incident coronary artery disease: a prospective, longitudinal cohort study. *Sci Adv*. 2023;9(38):eadf9037. doi:10.1126/sciadv.adf9037
61. Alfaddagh A, Kapoor K, Dardari ZA, et al. Omega-3 fatty acids, subclinical atherosclerosis, and cardiovascular events: implications for primary prevention. *Atherosclerosis*. 2022;353:11–19. doi:10.1016/j.atherosclerosis.2022.06.1018
62. Yokoi-Shimizu K, Yanagimoto K, Hayamizu K. Effect of docosahexaenoic acid and eicosapentaenoic acid supplementation on sleep quality in healthy subjects: a randomized, double-blinded, placebo-controlled trial. *Nutrients*. 2022;14(19):4136. doi:10.3390/nu14194136
63. Suzuki R, Sato Y, Fukaya M, et al. Energy metabolism profile of the effects of amino acid treatment on hepatocytes: phenylalanine and phenylpyruvate inhibit glycolysis of hepatocytes. *Nutrition*. 2021;82:111042. doi:10.1016/j.nut.2020.111042
64. Zhang Q, Chen S, Guo Y, et al. Phenylalanine diminishes M1 macrophage inflammation. *Sci China Life Sci*. 2023;66(12):2862–2876. doi:10.1007/s11427-022-2296-0
65. Wu Y, Ma Y, Li Q, et al. Multi-omics analysis reveals phenylalanine enhance mitochondrial function and hypoxic endurance via LKB1/AMPK activation. *J Transl Med*. 2024;22(1):920. doi:10.1186/s12967-024-05696-5
66. Tzoulaki I, Castagné R, Boulangé CL, et al. Serum metabolic signatures of coronary and carotid atherosclerosis and subsequent cardiovascular disease. *Eur Heart J*. 2019;40(34):2883–2896. doi:10.1093/eurheartj/ehz235
67. Zheng Y, Chen J, Macwan V, et al. S-acylation of ATGL is required for lipid droplet homoeostasis in hepatocytes. *Nat Metab*. 2024;6 (8):1549–1565. doi:10.1038/s42255-024-01085-w
68. Dai H, Wu R, Zhang J, et al. ZDHHC11B is decreased in lung adenocarcinoma and inhibits tumorigenesis via regulating epithelial-mesenchymal transition. *Cancer Med*. 2023;12(16):17212–17222. doi:10.1002/cam4.6345
69. Dzikiewicz-Krawczyk A, Kok K, Slezak-Prochazka I, et al. ZDHHC11 and ZDHHC11B are critical novel components of the oncogenic MYC-miR-150-MYB network in burkitt lymphoma. *Leukemia*. 2017;31(6):1470–1473. doi:10.1038/leu.2017.94
70. Liu E, Sun J, Yang J, et al. ZDHHC11 positively regulates NF-κB activation by enhancing TRAF6 oligomerization. *Front Cell Dev Biol*. 2021;9:710967. doi:10.3389/fcell.2021.710967
71. Liu Y, Zhou Q, Zhong L, et al. ZDHHC11 modulates innate immune response to DNA virus by mediating MITA-IRF3 association. *Cell Mol Immunol*. 2018;15(10):907–916. doi:10.1038/cmi.2017.146
72. Segal S, Arbel-Ganon L, Mazgaoker S, et al. Increase in Ca(2+)-Activated cAMP/PKA signaling prevents hydroxychloroquine-induced bradycardia of the cardiac pacemaker. *Front Physiol*. 2022;13:839140. doi:10.3389/fphys.2022.839140
73. Aranda-Domene R, Orenes-Piñero E, Arribas-Leal JM, et al. Evidence for a lack of inotropic and chronotropic effects of glucagon and glucagon receptors in the human heart. *Cardiovasc Diabetol*. 2023;22(1):128. doi:10.1186/s12933-023-01859-8

74. Hu XQ, Zhang L. Oxidative regulation of vascular Ca(v)1.2 channels triggers vascular dysfunction in hypertension-related disorders. *Antioxidants*. 2022;11(12). doi:10.3390/antiox11122432
75. Ali A, Memon Z, Hameed A, et al. Myricetin amplifies glucose-stimulated insulin secretion via the cAMP-PKA-Epac-2 signaling cascade. *Biomedicines*. 2025;13(6):1447. doi:10.3390/biomedicines13061447
76. Geisbuhler TP, Schwager TL, Ervin HD. 3-isobutyl-1-methylxanthine (IBMX) sensitizes cardiac myocytes to anoxia. *Biochem Pharmacol*. 2002;63 (11):2055–2062. doi:10.1016/S0006-2952(02)00901-2
77. Valerius T, Stockmeyer B, van Spriel AB, et al. FcalphaRI (CD89) as a novel trigger molecule for bispecific antibody therapy. *Blood*. 1997;90 (11):4485–4492. doi:10.1182/blood.V90.11.4485
78. You G, Zhao X, Liu J, et al. Machine learning-based identification of CYBB and FCAR as potential neutrophil extracellular trap-related treatment targets in sepsis. *Front Immunol*. 2023;14:1253833. doi:10.3389/fimmu.2023.1253833
79. Iakoubova OA, Tong CH, Chokkalingam AP, et al. Asp92Asn polymorphism in the myeloid IgA Fc receptor is associated with myocardial infarction in two disparate populations: CARE and WOSCOPS. *Arterioscler Thromb Vasc Biol*. 2006;26(12):2763–2768. doi:10.1161/01.ATV.0000247248.76409.8b
80. Wu J, Ji C, Xie F, et al. FcalphaRI (CD89) alleles determine the proinflammatory potential of serum IgA. *J Immunol*. 2007;178(6):3973–3982. doi:10.4049/jimmunol.178.6.3973
81. Desaki Y, Kanamaru Y, Monteiro R, et al. Fcα receptor type i and its association with atherosclerosis development. *Juntendo Iji Zasshi*. 2023;69 (3):231–239. doi:10.14789/jmj.JMJ23-0003-OA
82. Moskaleva NE, Shestakova KM, Kukharenko AV, et al. Target metabolome Profiling-Based machine learning as a diagnostic approach for cardiovascular diseases in adults. *Metabolites*. 2022;12(12):1185. doi:10.3390/metabo12121185
83. Kiens O, Taalberg E, Ivanova V, et al. The effect of obstructive sleep apnea on peripheral blood amino acid and biogenic amine metabolome at multiple time points overnight. *Sci Rep*. 2021;11(1):10811. doi:10.1038/s41598-021-88409-y
84. Gáspár R, Halmi D, Demján V, et al. Kynurenine pathway metabolites as potential clinical biomarkers in coronary artery disease. *Front Immunol*. 2021;12:768560. doi:10.3389/fimmu.2021.768560
85. Sebastiani J, Sabatelli A, McDonald MD. Mild hypoxia exposure impacts peripheral serotonin uptake and degradation in Gulf toadfish (Opsanus beta). *J Exp Biol*. 2022;225(13). doi:10.1242/jeb.244064
86. Dewan NA, Nieto FJ, Somers VK. Intermittent hypoxemia and OSA: implications for comorbidities. *Chest*. 2015;147(1):266–274. doi:10.1378/chest.14-0500
87. Wang Y, Liu G, Zhao Z, et al. The relationship between Type D personality with atherosclerotic plaque and cardiovascular events: the mediation effect of inflammation and kynurenine/tryptophan metabolism. *Front Cardiovasc Med*. 2022;9:986712. doi:10.3389/fcvm.2022.986712
88. Li Q, You Y, Zeng Y, et al. Associations between plasma tryptophan and indole-3-propionic acid levels and mortality in patients with coronary artery disease. *Am J Clin Nutr*. 2022;116(4):1070–1077. doi:10.1093/ajcn/nqac170
89. Xue H, Chen X, Yu C, et al. Gut microbially produced Indole-3-Propionic acid inhibits atherosclerosis by promoting reverse cholesterol transport and its deficiency is causally related to atherosclerotic cardiovascular disease. *Circ Res*. 2022;131(5):404–420. doi:10.1161/CIRCRESAHA.122.321253
90. Esposito A, Falace A, Wagner M, et al. Biallelic DMXL2 mutations impair autophagy and cause Ohtahara syndrome with progressive course. *Brain*. 2019;142(12):3876–3891. doi:10.1093/brain/awz326
91. Faronato M, Nguyen VT, Patten DK, et al. DMXL2 drives epithelial to mesenchymal transition in hormonal therapy resistant breast cancer through Notch hyper-activation. *Oncotarget*. 2015;6(26):22467–22479. doi:10.18632/oncotarget.4164
92. Yao G, Hu X, Song D, et al. Identification of Macrophage-Related biomarkers for abdominal aortic aneurysm through combined Single-Cell sequencing and machine learning. *J Inflamm Res*. 2024;17:11009–11027. doi:10.2147/JIR.S499593

Nature and Science of Sleep

Dovepress
Taylor & Francis Group

Publish your work in this journal

Nature and Science of Sleep is an international, peer-reviewed, open access journal covering all aspects of sleep science and sleep medicine, including the neurophysiology and functions of sleep, the genetics of sleep, sleep and society, biological rhythms, dreaming, sleep disorders and therapy, and strategies to optimize healthy sleep. The manuscript management system is completely online and includes a very quick and fair peer-review system, which is all easy to use. Visit http://www.dovepress.com/testimonials.php to read real quotes from published authors.

Submit your manuscript here: https://www.dovepress.com/nature-and-science-of-sleep-journal